Equilibrium and non-equilibrium properties of the layered magnetic models

A Synopsis (Approx. 5000 words)

Submitted by

Soham Chandra

Under the supervision of

Prof. Muktish Acharyya

In partial fulfillment for the award of the degree

Doctor of Philosophy in **Science**

Registration No.: R-18RS09110153

Date of Registration: 28.08.2019

Email: soham.rs@presiuniv.ac.in

Department of Physics

Faculty of Natural and Mathematical Sciences

Presidency University

Kolkata, India

2025

DECLARATION

I hereby declare that the dissertation entitled, "Equilibrium and non-equilibrium properties of the layered magnetic models" to be submitted for the degree of Doctor of Philosophy is my original work and the dissertation has not formed the basis for the award of any degree, diploma, associateship or fellowship of similar other titles. It has not been submitted to any other university or Institution for the award of any degree or diploma.

Date: 28.04.2025

Place: Kolkata

Soham Chandra

(Signature of the Candidate)

Contents

1 Introduction **6**

2 Literature Review **7**

3 Systems studied and aim of the investigations **7**

4 Methodology **8**

4.1 Recipe of the Metropolis Algorithm 9

5 Results, in brief, of equilibrium studies **10**

5.1 Systematics of Compensation in an Ising spin-1/2 Ising square trilayer 10

5.1.1 Results and Discussion 10

5.1.1.1 Analysis of Lattice morphology 10

5.1.1.2 IARRM and TICCT in ABA Composition 13

5.1.1.3 IARRM and TICCT in AAB Composition 13

5.2 Optimization of Compensation in a site-diluted Ising spin-1/2 square trilayer 13

5.2.1 Results and Discussion 14

5.2.1.1 Thermodynamic Response 14

5.2.1.2 Mathematical Modelling 14

5.2.1.3 Effect of Impurity on Phase diagram 15

6 Results, in brief, of nonequilibrium studies **18**

6.1 Effect of a Uniform Random External Magnetic Field with Spatiotemporal Variation on Compensation in Ising Spin-1/2 Trilayered Square Ferrimagnets 18

6.1.1 Results and Discussion 18

6.1.1.1 Shift in Compensation and Critical Temperatures 18

6.1.1.2 Field-Driven Absence of Compensation 22

6.2 Effect of a Gaussian Random External Magnetic Field with Spatiotemporal Variation on Compensation in Ising Spin-1/2 Trilayered Square Ferrimagnets 23

6.2.1 Results and Discussion 26

6.2.1.1 Magnetization vs. Temperature 26

6.2.1.2 Phase Diagram and Scaling 27

7 Conclusion and future directions **28**

References **28**

List of Figures

1 Miniaturised versions ($3 \times 4 \times 4$) of *pure* (a) *ABA* and (b) *AAB* square trilayered ferrimagnet with two types of theoretical atoms, A and B. Each of the sublattices of the ferrimagnetic systems is formed on square lattice. 8

2 Miniaturised versions ($3 \times 4 \times 4$) of *site-diluted*: (A) ABA-type and (B) AAB-type triangular trilayered Ising superlattices. Each of the sublattices of the ferrimagnetic systems are formed on triangular lattice. 8

3 The spin-density plots of ABA-type and AAB-type square trilayered Ising superlattices at $T \approx T_{crit}$ and $T \approx T_{comp}$. The actual simulations are carried out on a system with $N_{sites} = 3 \times 100 \times 100$. . . . 11

4 For ABA configurations: (a) plot of IARRM vs. controlling factors; (b) plot of ΔT vs. controlling factors. The actual simulations are carried out on a system with $N_{sites} = 3 \times 100 \times 100$. 12

5 For AAB configurations: (a) plot of IARRM vs. controlling factors; (b) plot of ΔT vs. controlling factors. The actual simulations are carried out on a system with $N_{sites} = 3 \times 100 \times 100$. 12

6 Phase diagrams of (a) AAB and (b) ABA configurations from the fitted formulae. In both the figures, rightside of the curves denote ferrimagnetic phase without compensation and left of the curves denote ferrimagnetic phase with compensation. 13

7 Plots of total magnetisation, M_{tot}, versus reduced temperature, T, with variable concentration of non-magnetic impurities, ρ, for: (a) ABA: $J_{AA}/J_{BB} = 0.20$ and $J_{AB}/J_{BB} = -0.20$; (b) ABA: $J_{AA}/J_{BB} = 0.84$ and $J_{AB}/J_{BB} = -0.84$; (c) AAB: $J_{AA}/J_{BB} = 0.20$ and $J_{AB}/J_{BB} = -0.20$; (d) AAB: $J_{AA}/J_{BB} = 0.84$ and $J_{AB}/J_{BB} = -0.84$. 15

8 The behaviour of the fitting quadratic polynomial or the variation of Compensation temperatures with an increase in the concentration of nonmagnetic impurities for a few representative cases, for an ABA configuration in (a) and (b) and for an AAB configuration in (c) and (d). 16

9 Plots of threshold concentration, ρ_T of spin-0 impurities versus Hamiltonian parameters: (a) ρ_T versus J_{AA}/J_{BB} and (b) ρ_T versus J_{AB}/J_{BB} , for an ABA configuration and (c) ρ_T versus J_{AA}/J_{BB} and (d) ρ_T versus J_{AB}/J_{BB} , for an AAB configuration. 16

10 Phase diagrams in the ($J_{AB}/J_{BB} \times J_{AA}/J_{BB}$) plane for: (a) ABA and (c) AAB configurations with concentration of nonmagnetic atoms acting as a parameter. The fractional area of the non-compensating region, $A(\rho)/A_{tot}$, as a function of concentration of non-magnetic impurities, ρ, for, (b) ABA configuration and (d) AAB configuration. 17

11 Verification of scaling behaviour of: (A) ABA-type and (B) AAB-type site-diluted square trilayered Ising superlattices. 17

12 Magnetic response of the trilayered system for a few selected cases with [(a)-(d)] for ABA and [(e)-(h)] for AAB. The shift of both the compensation (where it is present) and critical temperatures toward the low-temperature ends and shift of the magnetic behaviors among N, L, P, and Q, etc., type of ferrimagnetism, with increase in standard deviation of the uniform random external magnetic field, are clearly visible in all these plots. In (a) and (e) we witness the field-driven vanishing of compensation from $\sigma = 0.20$ and upwards. 19

13 For the ABA configuration: Lattice morphologies of the top layer (left); middle layer (middle), and the bottom layer (right) at $t = t_{morph} = 10^5$ MCS for a few selected coupling strengths and external field. The destruction of compensation in the cases (a) and (c) is due to the significant reduction of magnetic ordering in the top and bottom layers, i.e., surface layers. 20

14 For the AAB configuration: Lattice morphologies of the top layer (left), middle layer (middle), and bottom layer (right) at $t = t_{morph} = 10^5$ MCS for a few selected coupling strengths and external field. The destruction of compensation in the cases (a) and (c) is due to the significant reduction of magnetic ordering in the top and bottom layers, i.e., surface layers. 21
15 Phase diagram for the ABA trilayered ferrimagnetic system when (a) $\sigma = 0.52$, (b) $\sigma = 1.00$, and AAB trilayered ferrimagnetic system when (c) $\sigma = 0.52$ and (d) $\sigma = 1.00$, in presence of the uniform random external magnetic field. A: Compensation is absent; P: compensation is present. 22
16 Plots of magnitude of the area of the no-compensation islands versus standard deviation of the field (red) and the rate of increase in the magnitude of the area of the no-compensation islands versus standard deviation of the external uniform magnetic field (blue) for the (a) ABA and (b) AAB configurations. . 22
17 Magnetic response of the trilayered system for a few selected cases with [(a)-(d)] ABA. The shift of both the compensation (where it is present) and critical temperatures toward the low-temperature ends and shift of the magnetic behaviors among N, L, P, and Q, etc., type of ferrimagnetism, with increase in standard deviation of the Gaussian random external magnetic field, are clearly visible in all these plots. We witness the field-driven vanishing of compensation from $\sigma = 0.20$ and upwards. 24
18 Magnetic response of the trilayered system for a few selected cases with [(a)-(d)] AAB. The shift of both the compensation (where it is present) and critical temperatures toward the low-temperature ends and shift of the magnetic behaviors among N, L, P, and Q, etc., type of ferrimagnetism, with increase in standard deviation of the Gaussian random external magnetic field, are clearly visible in all these plots. We witness the field-driven vanishing of compensation from $\sigma = 0.20$ and upwards. 24
19 For the ABA configuration: Lattice morphologies of the top layer (left); middle layer (middle), and the bottom layer (right) at $t = t_{morph} = 10^5$ MCS for a few selected coupling strengths and external field. The destruction of compensation in the cases (a) and (c) is due to the significant reduction of magnetic ordering in the top and bottom layers, i.e., surface layers. 25
20 For the ABA configuration: Lattice morphologies of the top layer (left); middle layer (middle), and the bottom layer (right) at $t = t_{morph} = 10^5$ MCS for a few selected coupling strengths and external field. The destruction of compensation in the cases (a) and (c) is due to the significant reduction of magnetic ordering in the top and bottom layers, i.e., surface layers. 26
21 Phase diagram for the ABA trilayered ferrimagnetic system when (a) $\sigma = 0.52$, (b) $\sigma = 1.00$, and AAB trilayered ferrimagnetic system when (c) $\sigma = 0.52$ and (d) $\sigma = 1.00$, in presence of the Gaussian random external magnetic field. A: Compensation is absent; P: compensation is present. 27
22 Plots of magnitude of the area of the no-compensation islands versus standard deviation of the Gaussian random field (red) and the rate of increase in the magnitude of the area of the no-compensation islands versus standard deviation of the Gaussian random field (blue) for the (a) ABA and (b) AAB configurations. 27

List of Tables

1 Magnetic properties of some *Ising* magnets with the following abbreviations, **FM**: ferromagnetic (interlayer and intralayer); **AFM**: antiferromagnetic (interlayer and intralayer); **a-AFM**: the magnetic structure with interlayer antiferromagnetic coupling and intralayer ferromagnetic coupling; **f-L**: few-layer, **1L**: monolayer, and so on; $\perp$: out-of-plane. Unless specified, the properties are obtained from the bulk. 6
2 Table of scaling parameters of Equation [13] for ABA and AAB trilayer configurations. 17

1 Introduction

Physics has traditionally been divided into numerous categories, sub-categories, fields and sub-fields, which have grown in stature and increasingly diverged over the years in both, language and methodology. In this thesis, the approach towards description of various physical variables of magnetic systems relies entirely on established techniques of Statistical Mechanics. Since the finding of graphene [1] almost two decades ago, the family of two-dimensional (2D) layered materials have grown significantly. The first experimentally realized intrinsic magnetic order in the monolayer/few-layer limit was in 2D ferromagnets $CrGeTe_3$ [2] and CrI_3 [3, 4] in 2017, after which various 2D Magnetic Materials have been rapidly discovered and studied. The discovery of monolayer magnetic materials is generating considerable excitement within the 2D and Quasi-3D magnetic materials community because it enables fundamental studies of magnetism in the true 2D limit and applications based on the integration of mono and few magnetic layers into device structures [5]. The focus of this thesis is *trilayered magnets, described by Ising interactions* and a few prominent physical examples are compiled in Table [1].

Material	Magnetic ordering	Magnetic transition temperature	Easy Axis	Spin Model
Transition Metal Halides				
CrI_3 [3,4]	FM (Bulk/1L)	61 K (Bulk)	$\perp$	Ising
	a-AFM (f-L)	45 K (1L)	(Bulk/1L)	
FeI_2 [6]	AFM	9 K	$\perp$	Ising
$FeBr_2$ [6]	a-AFM	14 K	$\perp$	Ising
$FeCl_2$ [6]	a-AFM	24 K	$\perp$	Ising
Transition metal phosphorous tri-chalcogenides				
$FePS_3$ [7–9]	AFM (Bulk/1L)	118 K (Bulk)	$\perp$	Ising
	(zigzag-type)	104 K (1L)	(Bulk/1L)	
$FePSe_3$ [10,11]	AFM (zigzag-type)	119 K	$\perp$	Ising
Ternary tellurides				
$CrSiTe_3$ [12]	FM	32 K	$\perp$	Ising
Fe_3GeTe_2 [13]	FM (Bulk/1L)	230 K (Bulk)	$\perp$	Ising
		130 K (1L)	(Bulk/1L)	

Table 1: Magnetic properties of some *Ising* magnets with the following abbreviations, **FM**: ferromagnetic (interlayer and intralayer); **AFM**: antiferromagnetic (interlayer and intralayer); **a-AFM**: the magnetic structure with interlayer antiferromagnetic coupling and intralayer ferromagnetic coupling; **f-L**: few-layer, **1L**: monolayer, and so on; $\perp$: out-of-plane. Unless specified, the properties are obtained from the bulk.

Let's review key points favouring investigations into layered magnetic materials [14]:
(a) For these layered materials, the surface-to-volume ratio is higher.
(b) Saturated van der Waals bonds make the physical properties tunable by external perturbations [15].
(c) Heterostructure interfaces have weaker interfacial coupling; interlayer twist-angles are controllable.
(d) Absence of lattice mismatch makes coupling to other functional 2D materials possible.
(e) Exchange interactions are highly anisotropic. In-plane exchange is usually stronger than out-of-plane exchange interactions.
(f) Spin-states can be manipulated by critical fluctuations.

Despite rapid development in the last two decades, there are stil a lot of untapped ideas in this still-evolving area of material science, from the perspectives of both theorists and experimentalists.

2 Literature Review

Since the discovery of ferrimagnetism in 1948, a ferrimagnet is frequently modelled as a combination of two or more magnetic substructures, such as sublattices, sublayers, or subsets of atoms [16, 17]. The compensation point (T_{comp}) is the temperature at which the resulting magnetization disappears below the critical temperature. The emergence of a compensation point results from the distinct temperature dependences of the sublattice magnetizations, which cause the magnetic moments of the sublattices to fully compensate one another at $T = T_{comp}$. The magnetic compensation phenomena, in trilayered ferrimagnets of ABA and AAB types, occupy lion share of attention of this thesis. In the available literature, there are limited instances of trilayered superlattices being investigated for magnetic compensation. These types of systems are yet to receive the same level of extensive interest compared to bilayers and multiple layers. The analysis of a spin-1/2 Ising square trilayered superlattice through both the Mean-Field Approximation (MFA) and the EFA [18] and Monte Carlo Simulation [19] demonstrated that, a single spin system with an odd number of layers can exhibit a ferrimagnetic phase featuring compensation without the need for site dilution.

In this thesis, our focus lies on this specific kind of trilayered ferrimagnetic system (Figures 1 and 2). At the compensation point, the bulk magnetization is zero while *the individual layers remain magnetically ordered* [17]. This contrasts with single-spin bilayers [20, 21] and multilayers [22, 23], where dilution becomes a prerequisite for a non-zero compensation temperature. Consequently, our investigation centers on a three-layered spin-1/2 Ising model comprising two distinct types of atoms (A and B) with each layer exclusively consisting of one type of atom. Our primary objective is to establish the criteria for the emergence of the compensation effect and ascertain the influence of each parameter on its occurrence. Although a prior analysis of this model has been conducted in Reference [18] using mean-field and effective-field approximations (MFA and EFA), it's noteworthy that while mean-field approaches often yield quick and qualitatively accurate solutions for most models, this approach may not consistently capture the precise physical behaviors of certain low-dimensional systems. One way around these difficulties or issues is performing Monte Carlo simulations on these magnetic systems.

3 Systems studied and aim of the investigations

The pristine trilayered Ising ferrimagnet, on square monolayers in two configurations: ABA and AAB (Figure [1]), comprises two types of atoms: A and B. Intra-layer interactions between like atoms ($A - A; B - B$) is ferromagnetic and interactions between unlike atoms ($A - B$) is antiferromagnetic. When the above trilayered configurations are site-diluted in the A-layers, the systems look like the ones depicted in Figure [2]. Monte Carlo simulations employing the Metropolis algorithm [24] are used to study magnetization, phase transitions, and compensation behavior. In [25, 26], the systematics of compensation is proposed of pristine trilayered square ferrimagnets of type ABA and AAB. In [27], the systematics and scaling relations are proposed for a site-diluted trilayered square ferrimagnet, highlighting randomness in layer compositions. Next, the impact of external random magnetic fields, has been investigated by applying a uniform random [28] and Gaussian random [29] magnetic field onto the pristine trilayered configurations.

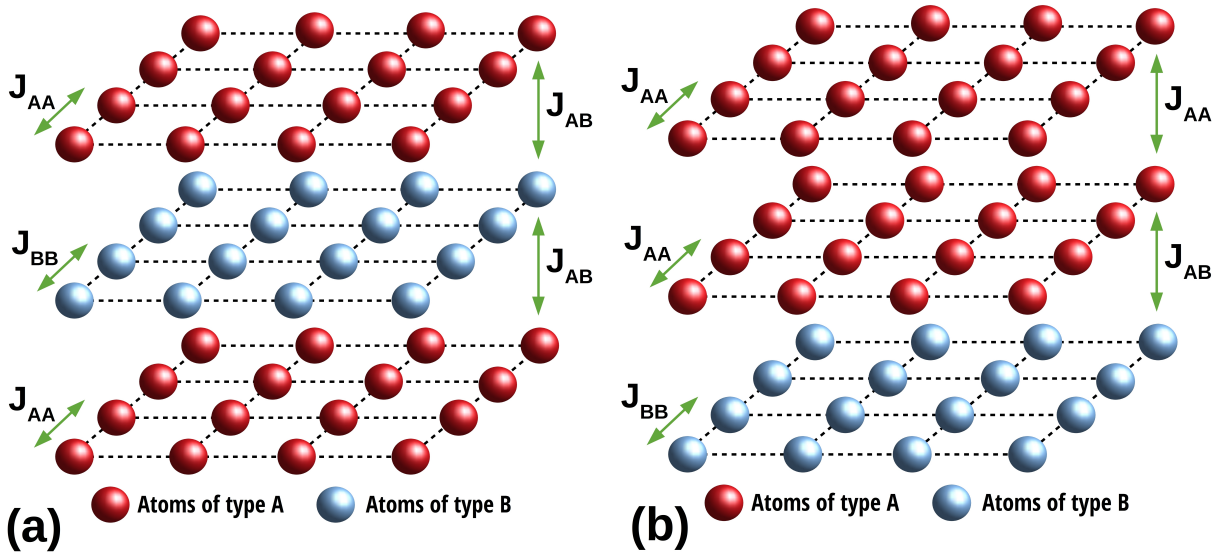

Figure 1: Miniaturised versions $(3 \times 4 \times 4)$ of *pure* (a) ABA and (b) AAB square trilayered ferrimagnet with two types of theoretical atoms, A and B. Each of the sublattices of the ferrimagnetic systems is formed on square lattice.

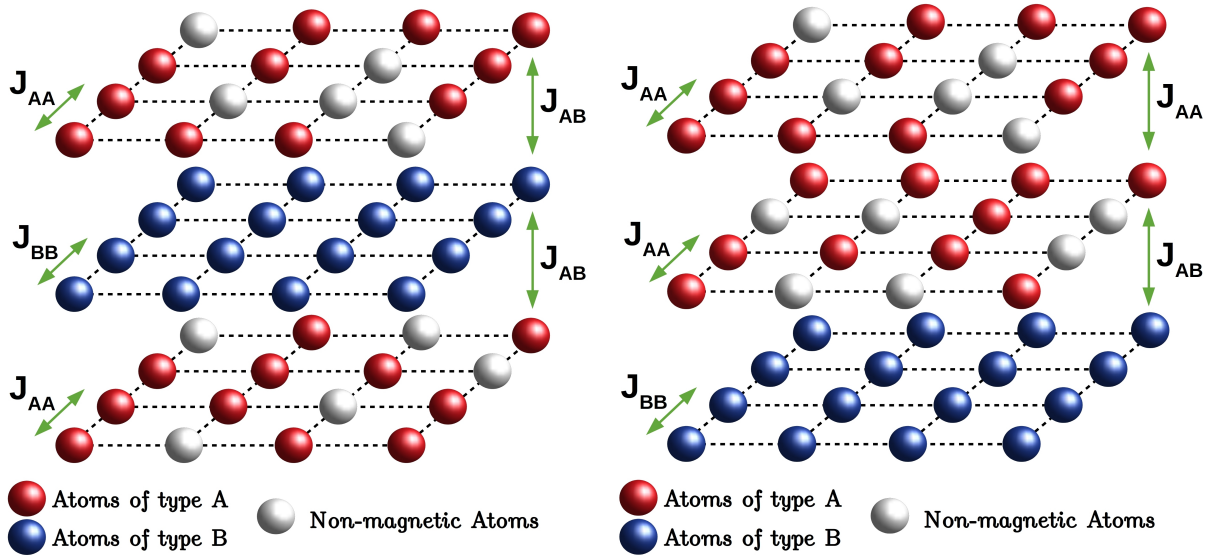

Figure 2: Miniaturised versions $(3 \times 4 \times 4)$ of *site-diluted*: (A) ABA-type and (B) AAB-type triangular trilayered Ising superlattices. Each of the sublattices of the ferrimagnetic systems are formed on triangular lattice.

4 Methodology

The Ising model, named after Ernst Ising, who first examined it in 1924, has played an important role in the development of statistical physics and quantum field theory [30], and is arguably the simplest and most celebrated model to conceive the magnetic phase transition is the spin-1/2 Ising model [31]. A lattice of discrete spins, having magnetic moments of ± 1, is historically considered in this model [32] with only the nearest neighbor interactions. In two dimensions, the Ising model on the square lattice has $L \times L$ spins in which each spin interacts with its four nearest neighbours, *two along each of the perpendicular directions*, and the most familiar Ising model is ferromagnetic with a constant exchange energy J. In the presence of an external magnetic field, h, the model Hamiltonian is written as:

$$H = -J \sum_{<i,j>} S_i^z S_j^z - h \sum_i S_i^z \tag{1}$$

where $< ij >$ represents distinct nearest-neighbor pairs only. Here, the S_i and S_j's are the "spin" variables which can take values ± 1 and reside on the sites of a lattice, and h is the longitudinal field that couples to each spin. Replacing the value of spin-projections $\pm 1/2$ by ± 1 is termed as pseudo-spin formalism and this rescales the energy scale of the system. In the absence of the external field, h, the model has a discrete up-down symmetry (Z_2) and undergoes a temperature-driven, second order phase transition from a symmetry-broken ferromagnetic phase with a non-zero spontaneous magnetization to the symmetric paramagnetic phase with zero magnetization. In general, the exchange coupling can be site- or spin-specific. So, the Hamiltonian of Equation [1] can be easily generalized into:

$$H = -\sum_{<i,j>} J_{ij} S_i^z S_j^z - h \sum_i S_i^z \tag{2}$$

The standard ferromagnetic Ising model is described by a nearest-neighbor interaction with $J_{ij} = J > 0$, while $J_{ij} = J < 0$ describes the antiferromagnetic Ising model.

4.1 Recipe of the Metropolis Algorithm

An important aspect of the Monte Carlo algorithms is the *ergodicity*.

A process or algorithm is said to satisfy ergodicity, if any state can be obtained from any other state, provided a sufficiently long simulation time is given to sample all the possible states of a system. This property must be satisfied to get a useful algorithm. As such, from any state m, there must be a path, no matter how long it takes, to any other state n in the Markov chain and the converse is also true.

As a summary to the usage of the Metropolis algorithm [24] in Monte Carlo simulations, the following steps are done for one application of the algorithm:

1. Choose an initial state, m .
2. Calculate the energy of the system, E_m.
3. Randomly pick a spin on the lattice.
4. Calculate the energy of the system, E_n, if the spin is flipped.
5. Calculate the difference in energy, $\Delta E = E_n - E_m$, between this state (after flipping) and the previous one.
6. If $\Delta E < 0$, the spin is flipped. Otherwise, the next step is followed.
7. Calculate the Boltzmann weight, $w = e^{-\beta \Delta E}$.
8. Generate a random number $0 < r < 1$.
9. If $r < w$, flip the spin. If not, no change is made.
10. Go to step 2.

The random number r must be uniformly selected between $[0, 1]$, and subsequent random values must be uncorrelated.

5 Results, in brief, of equilibrium studies

5.1 Systematics of Compensation in an Ising spin-1/2 Ising square trilayer

This study investigates the thermodynamic properties of a spin-1/2 Ising trilayered ferrimagnetic systems (Figure 1) on a square Bravais lattice using Monte Carlo (MC) simulations. The study focuses on two proposed variables, the Inverse Absolute of Reduced Residual Magnetisation (IARRM) and the temperature interval between the compensation and critical temperatures (TICCT). With all of the S^zs being z components of spin moments on lattice sites, the Hamiltonian using nearest neighbour Ising mechanics [32] is as follows:

$$H_{ABA} = -J_{AA}[\sum_{<t,t'>} S_t^z S_{t'}^z + \sum_{<b,b'>} S_b^z S_{b'}^z] - J_{BB} \sum_{<m,m'>} S_m^z S_{m'}^z - J_{AB}[\sum_{<t,m>} S_t^z S_m^z + \sum_{<m,b>} S_m^z S_b^z] \quad (3)$$

$$H_{AAB} = -J_{AA}[\sum_{<t,t'>} S_t^z S_{t'}^z + \sum_{<m,m'>} S_m^z S_{m'}^z] - J_{BB} \sum_{<b,b'>} S_b^z S_{b'}^z - J_{AA} \sum_{<t,m>} S_t^z S_m^z - J_{AB} \sum_{<m,b>} S_m^z S_b^z \quad (4)$$

where J_{BB} (on the B-layer) and J_{AA} (on the A-layers) are the intra-layer ferromagnetic coupling strengths between the nearest neighbours. J_{AB} represents the inter-layer antiferromagnetic coupling strengths. Based on the nature of magnetic interactions, $J_{AA} > 0$, $J_{BB} > 0$, and $J_{AB} < 0$. $< t, t' >$, $< m, m' >$, and $< b, b' >$ are the nearest neighbour summation indices for the top, mid, and bottom layers, respectively. Similarly, $< t, m >$ and $< m, b >$ imply summations over nearest-neighbor pairs in vertically adjacent layers. The governing parameters would be the ferromagnetic coupling ratio J_{AA}/J_{BB} and the antiferromagnetic coupling ratio J_{AB}/J_{BB}. We would also assume that J_{BB} is the dominant coupling strength of them all and set it to unity.

Monte Carlo simulations using the Metropolis single spin-flip algorithm were employed to analyze the systems. The system, modeled on a square lattice of size $3 \times 100 \times 100$. Simulations were performed over 10^5 Monte Carlo steps, with 5×10^4 steps for equilibration and 5×10^4 steps for thermal averaging. The relative interaction strengths were varied in the range $J_{AA}/J_{BB} \in [0.1, 1.0]$ and $J_{AB}/J_{BB} \in [-1.0, -0.1]$. The compensation temperature and critical temperature were determined using magnetization curves and fluctuation peaks.

5.1.1 Results and Discussion

5.1.1.1 Analysis of Lattice morphology

For ABA systems, at the compensation temperature, T_{comp}, the middle layer (B) magnetically saturates in the opposite direction to the top (A) and bottom (A) layers. At the critical temperature, spin clusters are more prominent in the middle layer, influencing the transition behavior (Refer to Panel 1 and Panel 2 of Figure [3]).

For AAB systems: At the compensation temperature, the bottom layer (B) is magnetically saturated in the opposite direction to the top (A) and middle (A) layers. At the critical temperature, larger spin clusters form in the bottom layer, leading to greater absolute magnetization than the other layers (Refer to Panel 3 and Panel 4 of Figure [3]).

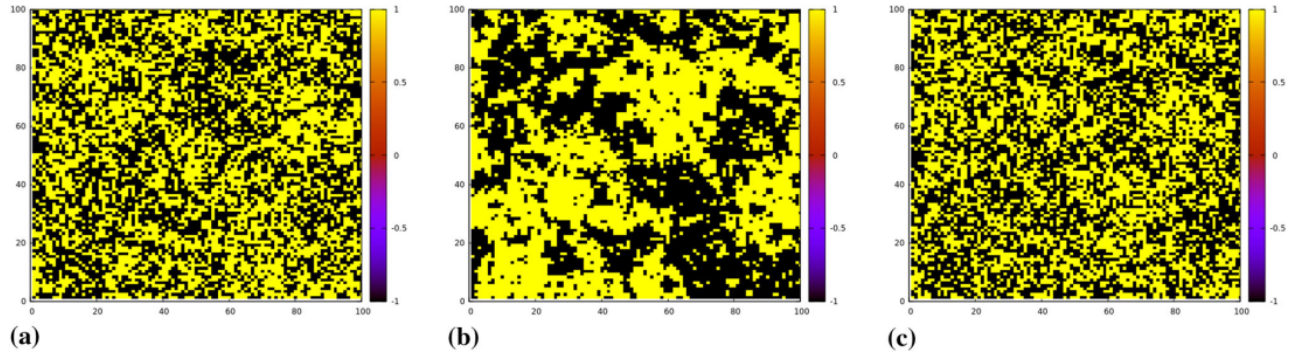

Panel 1: For the ABA stacking, lattice morphology of (a) top layer, (b) mid layer and (c) bottom layer with $(J_{AA}/J_{BB} = 0.3$ and $J_{AB}/J_{BB} = -0.4)$ at $T_{crit} = 2.6$ with $M_t = -2.91 \times 10^{-3}$, $M_m = 1.23 \times 10^{-2}$, $M_b = -3.07 \times 10^{-3}$

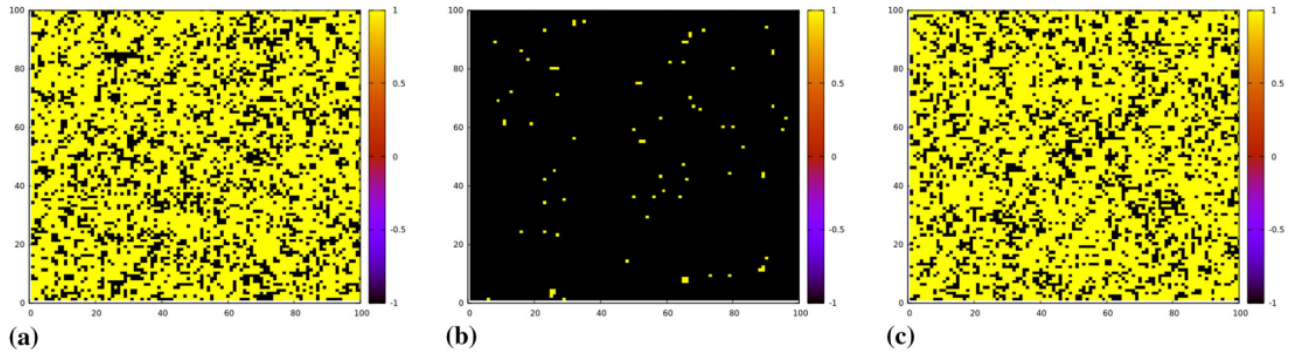

Panel 2: For the ABA stacking, lattice morphology of (a) top layer, (b) mid layer and (c) bottom layer with $(J_{AA}/J_{BB} = 0.3$ and $J_{AB}/J_{BB} = -0.4)$ at $T_{comp} \approx T = 1.7$ with $M_t = -0.48$, $M_m = 0.98$, $M_b = -0.48$

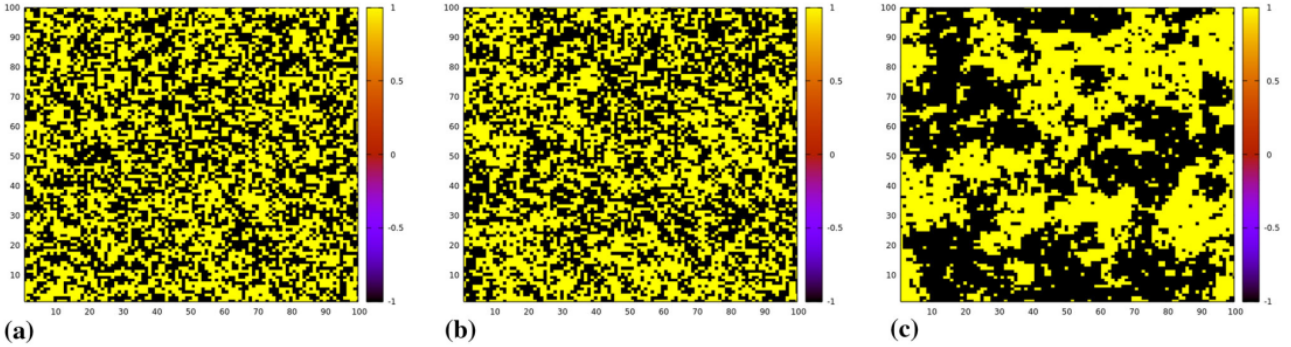

Panel 3: For the AAB stacking, lattice morphology of (a) top layer, (b) mid layer and (c) bottom layer with $(J_{AA}/J_{BB} = 0.3$ and $J_{AB}/J_{BB} = -0.4)$ at $T_{crit} = 2.4$ with $M_t = -0.01$, $M_m = -0.05$, $M_b = 0.17$

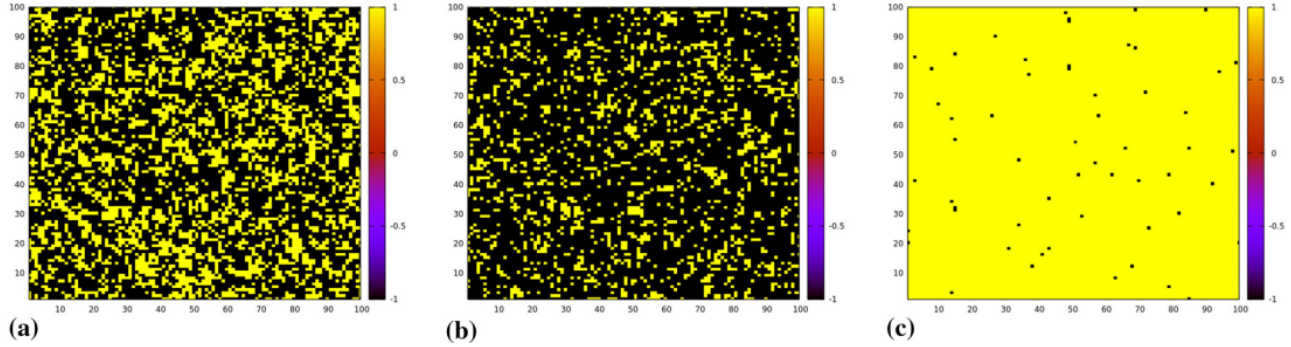

Panel 4: For the AAB stacking, lattice morphology of (a) top layer, (b) mid layer and (c) bottom layer with $(J_{AA}/J_{BB} = 0.3$ and $J_{AB}/J_{BB} = -0.4)$ at $T_{comp} \approx T = 1.5$ with $M_t = -0.32$, $M_m = -0.62$, $M_b = 0.99$

Figure 3: The spin-density plots of ABA-type and AAB-type square trilayered Ising superlattices at $T \approx T_{crit}$ and $T \approx T_{comp}$. The actual simulations are carried out on a system with $N_{sites} = 3 \times 100 \times 100$.

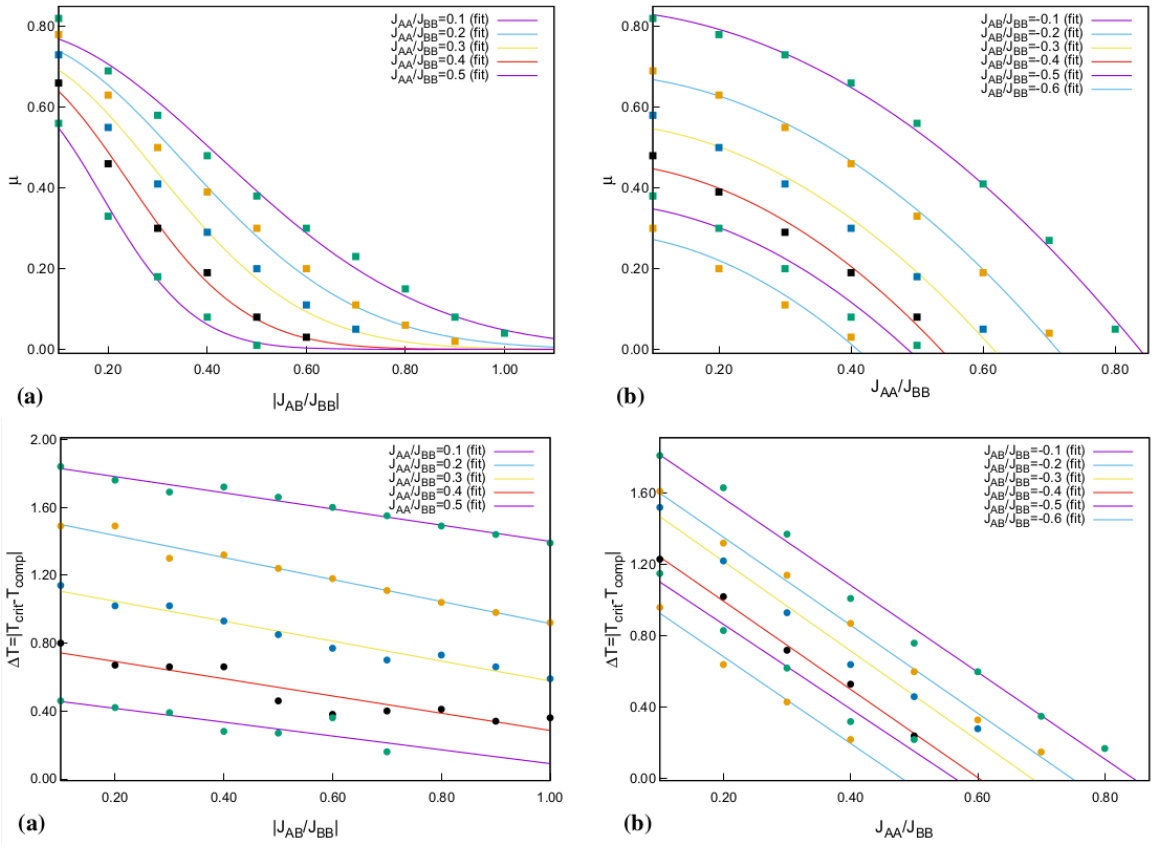

Figure 4: For ABA configurations: (a) plot of IARRM vs. controlling factors; (b) plot of ΔT vs. controlling factors. The actual simulations are carried out on a system with $N_{sites} = 3 \times 100 \times 100$.

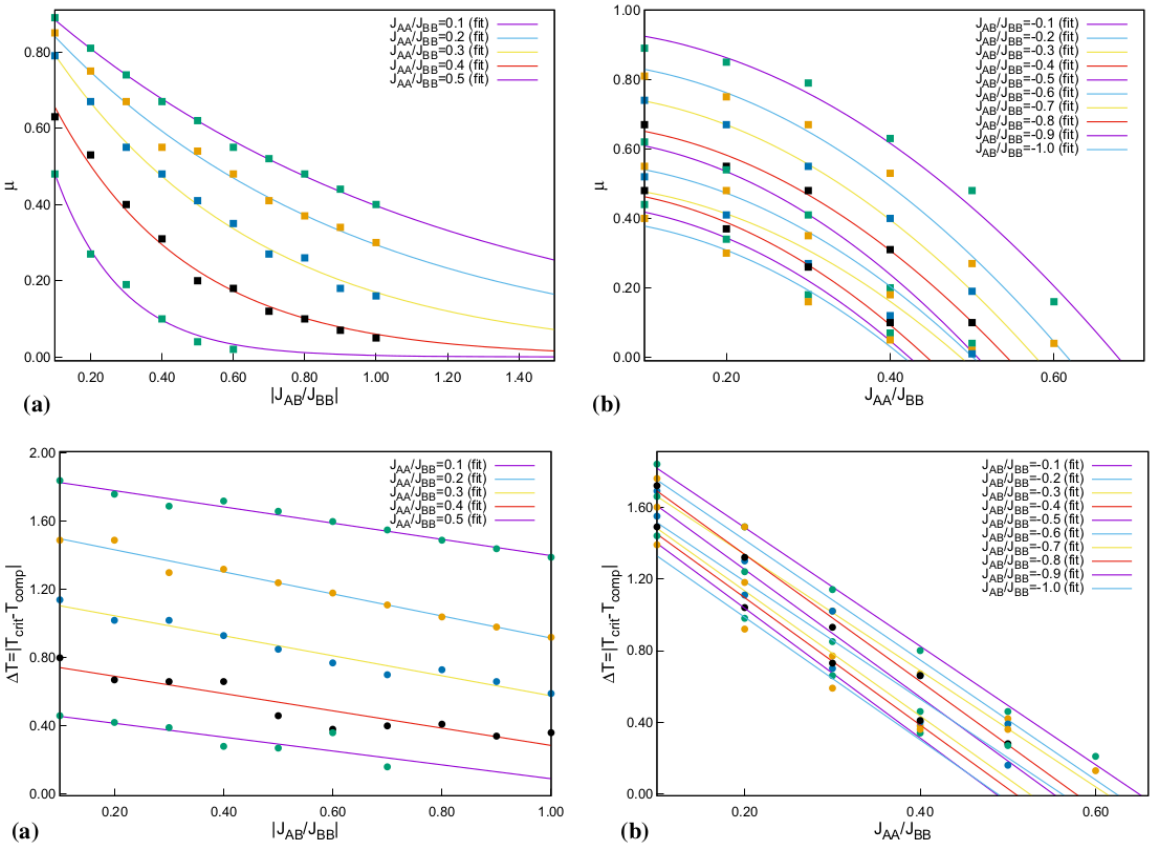

Figure 5: For AAB configurations: (a) plot of IARRM vs. controlling factors; (b) plot of ΔT vs. controlling factors. The actual simulations are carried out on a system with $N_{sites} = 3 \times 100 \times 100$.

5.1.1.2 IARRM and TICCT in ABA Composition

For ABA systems, **Inverse Absolute of Reduced Residual Magnetisation (IARRM)**, follows the proposed equation (in Figure [4](a) with, b_1, b_2, b_3, and b_4 being the fitting coefficients):

$$\left|\frac{M_{max,int}}{M_{sat}}\right|^2_{ABA} = \mu^2_{ABA}\left(\frac{J_{AA}}{J_{BB}}, \frac{J_{AB}}{J_{BB}}\right) = b_1 e^{-b_2(J_{AB}/J_{BB})^2}\left[b_3 - b_4\left(\frac{J_{AA}}{J_{BB}}\right)^2\right] \tag{5}$$

Variation of **Temperature Interval (ΔT) between Critical and Compensation temperatures (TICCT)**, is modeled as (in Figure [4](b) with, b_5, b_6, b_7, and b_8 being the fitting coefficients):

$$|T_{crit} - T_{comp}|^2_{ABA} = \Delta T^2_{ABA}\left(\frac{J_{AA}}{J_{BB}}, \frac{J_{AB}}{J_{BB}}\right) = \left[-b_5\left|\frac{J_{AB}}{J_{BB}}\right| + b_6\right]\left[-b_7\left(\frac{J_{AA}}{J_{BB}}\right) + b_8\right] \tag{6}$$

5.1.1.3 IARRM and TICCT in AAB Composition

For AAB systems, **Inverse Absolute of Reduced Residual Magnetisation (IARRM)**, follows the proposed equation (in Figure 5(a) with, a_1, a_2, a_3, and a_4 being the fitting coefficients):

$$\left|\frac{M_{max,int}}{M_{sat}}\right|^2_{AAB} = \mu^2_{AAB}\left(\frac{J_{AA}}{J_{BB}}, \frac{J_{AB}}{J_{BB}}\right) = a_1 e^{-a_2|J_{AB}/J_{BB}|}\left(a_3 - a_4\left(\frac{J_{AA}}{J_{BB}}\right)^2\right) \tag{7}$$

Variation of **Temperature Interval (ΔT) between Critical and Compensation temperatures (TICCT)**, is modeled as (in Figure [5](b) with, a_5, a_6, a_7, and a_8 being the fitting coefficients):

$$|T_{crit} - T_{comp}|^2_{AAB} = \Delta T^2_{AAB}\left(\frac{J_{AA}}{J_{BB}}, \frac{J_{AB}}{J_{BB}}\right) = \left[-a_5\left|\frac{J_{AB}}{J_{BB}}\right| + a_6\right]\left[-a_7\left(\frac{J_{AA}}{J_{BB}}\right) + a_8\right] \tag{8}$$

The phase diagrams in the Hamiltonian parameter space, by analysing IARRM and TICCT, are given in Figure [6]

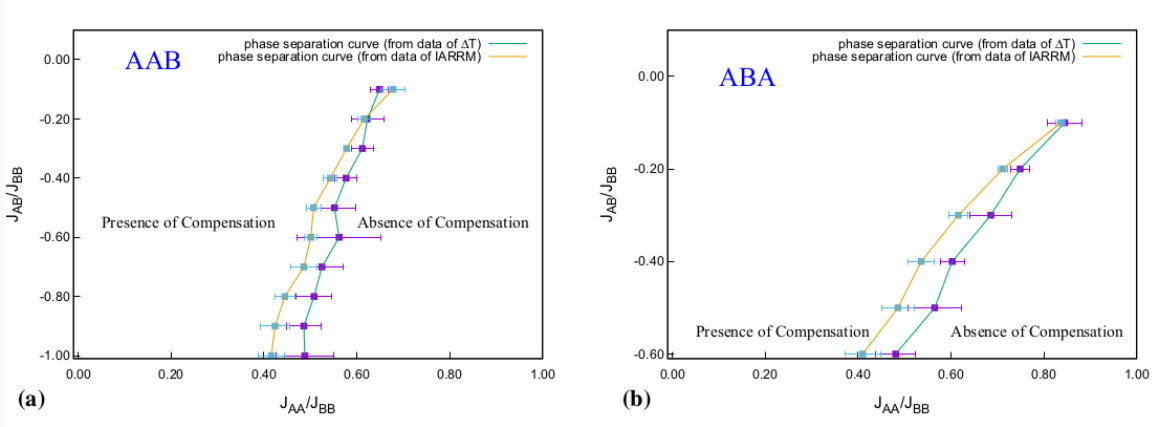

Figure 6: Phase diagrams of (a) AAB and (b) ABA configurations from the fitted formulae. In both the figures, rightside of the curves denote ferrimagnetic phase without compensation and left of the curves denote ferrimagnetic phase with compensation.

5.2 Optimization of Compensation in a site-diluted Ising spin-1/2 square trilayer

In layered ferrimagnets, the interplay of ferromagnetic and antiferromagnetic interactions lead to compensation phenomenon, which is crucial for applications in magneto-optics, spintronics, and data storage [33, 34]. The work, in [27], focuses on a trilayered triangular Ising model with site dilution to explore how nonmagnetic impurities affect the magnetic and thermodynamic properties. The system

consists of three square monolayers stacked in either an ABA or AAB configuration (Figure 2). We would write the interacting Hamiltonians as:

$$\begin{aligned} H_{ABA} = & - J_{AA}[\sum_{<t,t'>}(\xi_t S_t^z)(\xi_{t'} S_{t'}^z) + \sum_{<b,b'>}(\xi_b S_b^z)(\xi_{b'} S_{b'}^z)] - J_{BB}\sum_{<m,m'>} S_m^z S_{m'}^z \\ & - J_{AB}[\sum_{<t,m>}(\xi_t S_t^z) S_m^z + \sum_{<m,b>} S_m^z(\xi_b S_b^z)] \end{aligned} \tag{9}$$

$$\begin{aligned} H_{AAB} = & - J_{AA}[\sum_{<t,t'>}(\xi_t S_t^z)(\xi_{t'} S_{t'}^z) + \sum_{<m,m'>}(\xi_m S_m^z)(\xi_{m'} S_{m'}^z)] - J_{BB}\sum_{<b,b'>} S_b^z S_{b'}^z \\ & - J_{AA}\sum_{<t,m>}(\xi_t S_t^z)(\xi_m S_m^z) - J_{AB}\sum_{<m,b>}(\xi_m S_m^z) S_b^z \end{aligned} \tag{10}$$

The configurational averages of the occupancy probability of A-atoms for the ABA variant are $\bar{\xi_t} = \bar{\xi_b} = (1-\rho)$, and for the AAB variant, they are $\bar{\xi_t} = \bar{\xi_m} = (1-\rho)$,with ρ : concentration of nonmagnetic atoms. The top and bottom layers don't interact with each other out of plane. The system consists of 100×100 spins per layer with periodic boundary conditions in-plane and open boundary conditions along the vertical axis. The critical and compensation temperatures are determined using Binder's fourth order magnetization cumulant analysis [35].

5.2.1 Results and Discussion

5.2.1.1 Thermodynamic Response

Magnetization curves indicate that increasing impurity concentration shifts the compensation temperature toward lower values while maintaining second-order phase transitions. Critical temperatures remain relatively stable, highlighting the robustness of the system's magnetic ordering (Figure 7). This behavior suggests that the system retains its overall ferrimagnetic character, despite disorder-induced variations in sublayer magnetization profiles. The specific heat exhibits a pronounced peak at the critical temperature, confirming the second-order nature of the transition. Meanwhile, magnetic susceptibility shows a peak about the compensation temperature, highlighting the strong influence of site dilution on the balance of sublattice magnetization.

5.2.1.2 Mathematical Modelling

The variation of compensation temperature with impurity concentration follows a quadratic relation (Figure [8]). For ABA:

$$T_{comp,ABA}\left(\rho, \frac{J_{AA}}{J_{BB}}, \frac{J_{AB}}{J_{BB}}\right) = p_1\rho^2 + q_1\rho + r_1 \tag{11}$$

and for AAB:

$$T_{comp,AAB}\left(\rho, \frac{J_{AA}}{J_{BB}}, \frac{J_{AB}}{J_{BB}}\right) = p_2\rho^2 + q_2\rho + r_2 \tag{12}$$

The coefficients, namely, $p_i \equiv p_i(J_{AA}/J_{BB}, J_{AB}/J_{BB})$; $q_i \equiv q_i(J_{AA}/J_{BB}, J_{AB}/J_{BB})$; and $r_i \equiv r_i(J_{AA}/J_{BB}, J_{AB}/J_{BB})$ with $i \in \{1, 2\}$ explicitly depend upon the reduced coupling strengths, i.e. J_{AA}/J_{BB}, and J_{AB}/J_{BB}. Additionally, we analyze how the threshold impurity concentration (ρ_T) depends on the Hamiltonian parameters (Figure [9]).

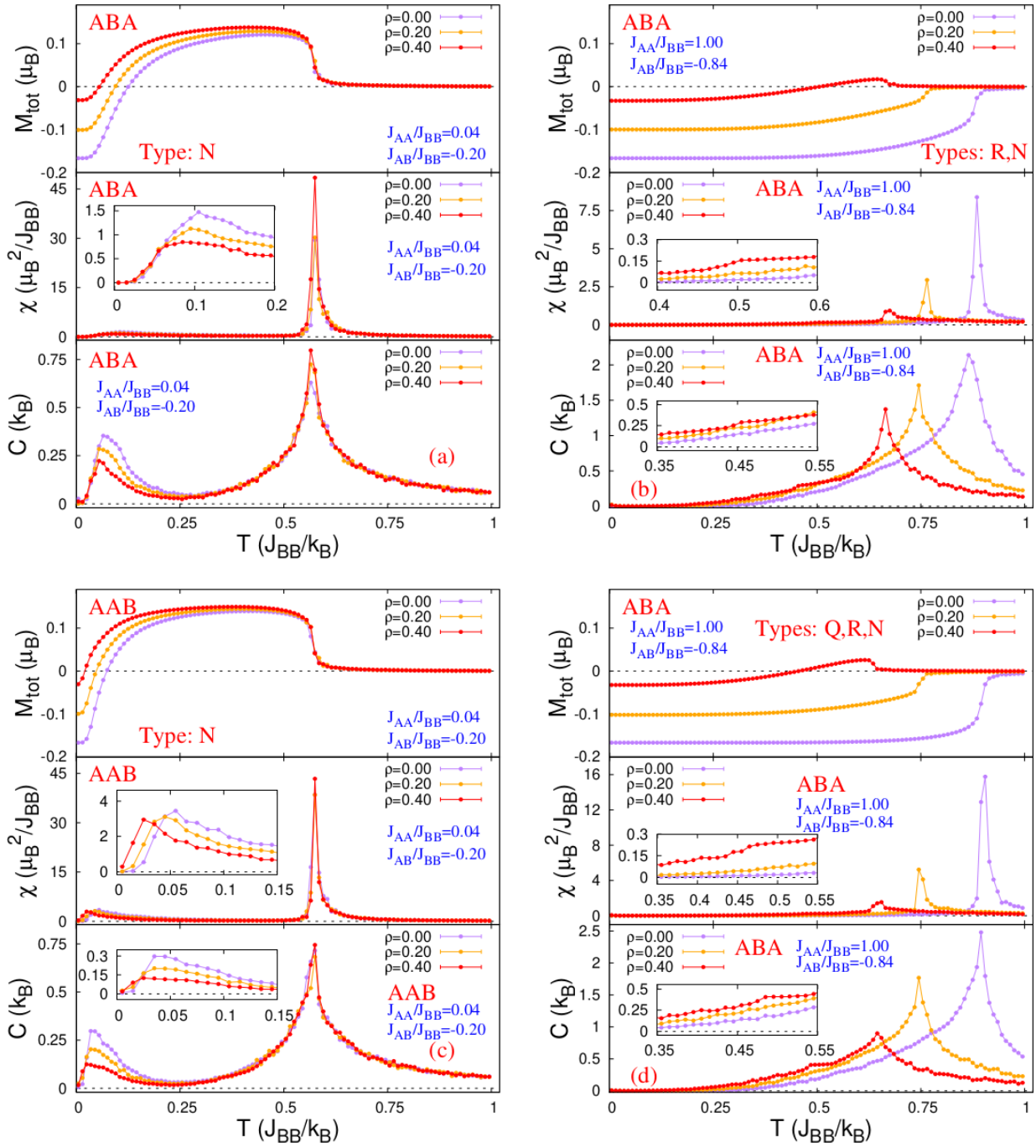

Figure 7: Plots of total magnetisation, M_{tot}, versus reduced temperature, T, with variable concentration of non-magnetic impurities, ρ, for: (a) ABA: $J_{AA}/J_{BB} = 0.20$ and $J_{AB}/J_{BB} = -0.20$; (b) ABA: $J_{AA}/J_{BB} = 0.84$ and $J_{AB}/J_{BB} = -0.84$; (c) AAB: $J_{AA}/J_{BB} = 0.20$ and $J_{AB}/J_{BB} = -0.20$; (d) AAB: $J_{AA}/J_{BB} = 0.84$ and $J_{AB}/J_{BB} = -0.84$.

5.2.1.3 Effect of Impurity on Phase diagram

Dilution introduced disorder, enables the creation of new compensation points. For certain combinations of dilution percentage and coupling strengths, compensation points emerge where they were previously *absent in the pure system.* The phase diagrams in Figure [10] illustrate how the non-compensating region shrinks with increasing impurity concentration. While examining the dynamics of sublattice magnetizations, the A-layers, being diluted, experience a weakened net magnetic moment, while the B-layer remains unaffected. As a result, for intermediate impurity concentrations, the net magnetization of the system cancels out at lower temperatures, leading to a well-defined compensation

point in site-diluted systems.

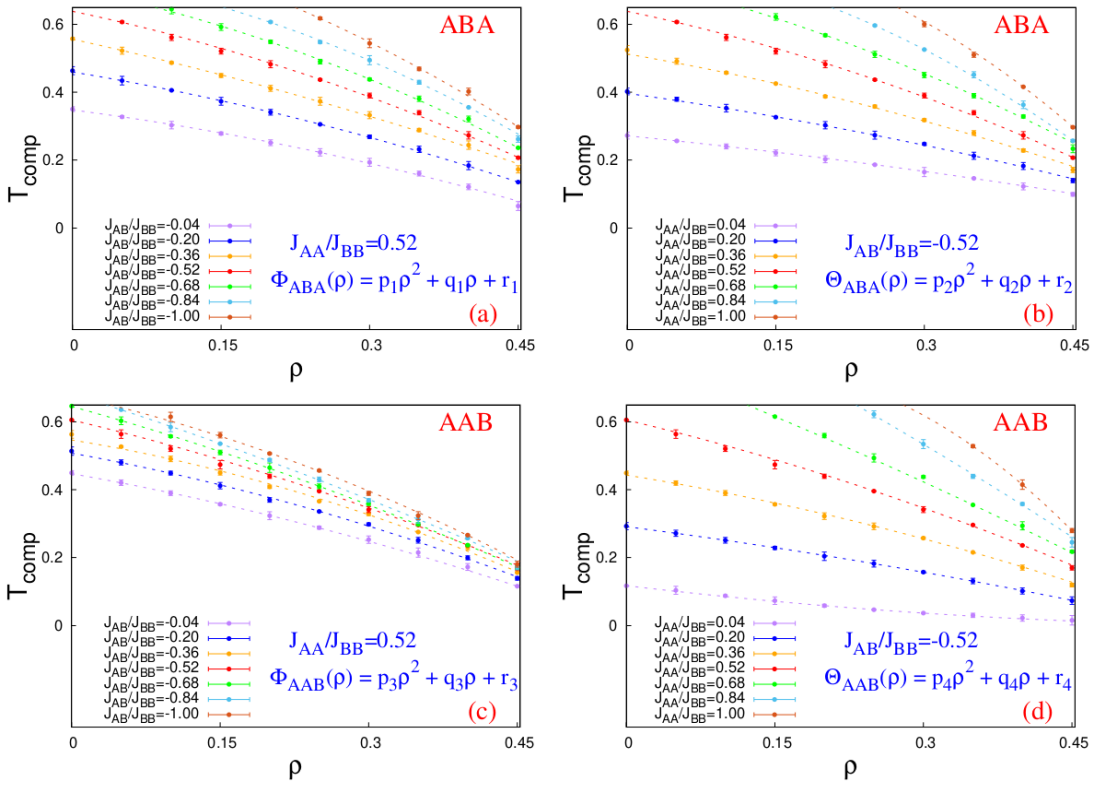

Figure 8: The behaviour of the fitting quadratic polynomial or the variation of Compensation temperatures with an increase in the concentration of nonmagnetic impurities for a few representative cases, for an ABA configuration in (a) and (b) and for an AAB configuration in (c) and (d).

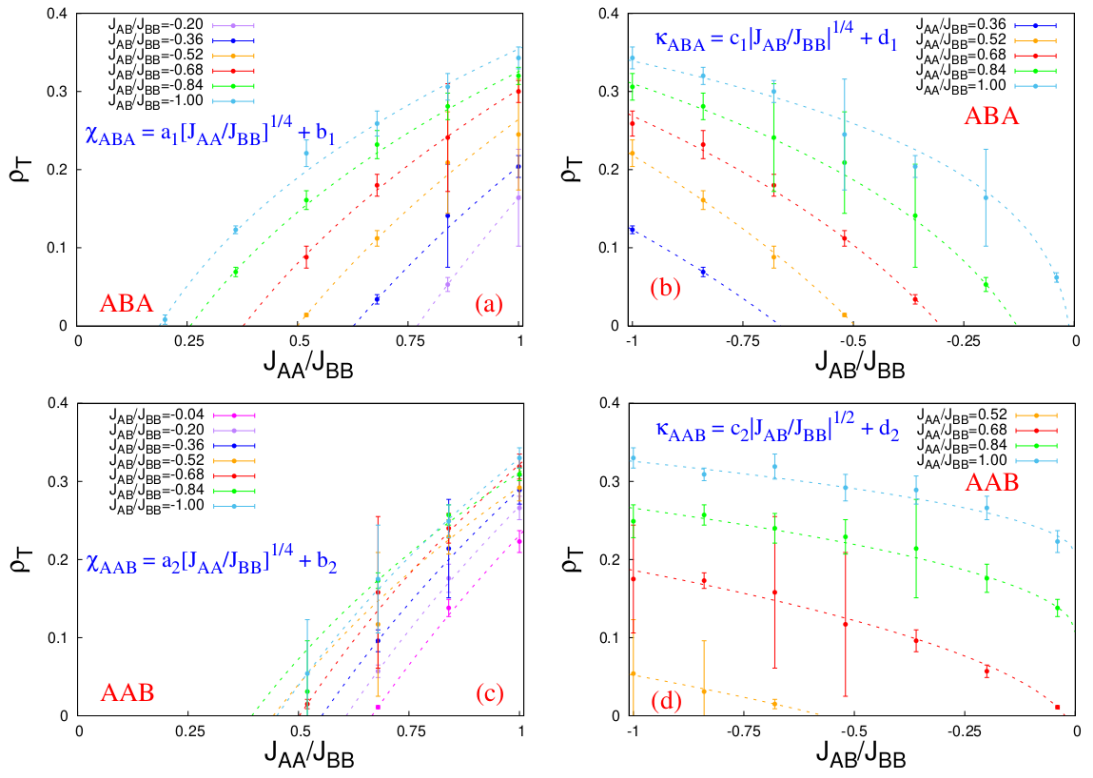

Figure 9: Plots of threshold concentration, ρ_T of spin-0 impurities versus Hamiltonian parameters: (a) ρ_T versus J_{AA}/J_{BB} and (b) ρ_T versus J_{AB}/J_{BB} , for an ABA configuration and (c) ρ_T versus J_{AA}/J_{BB} and (d) ρ_T versus J_{AB}/J_{BB} , for an AAB configuration.

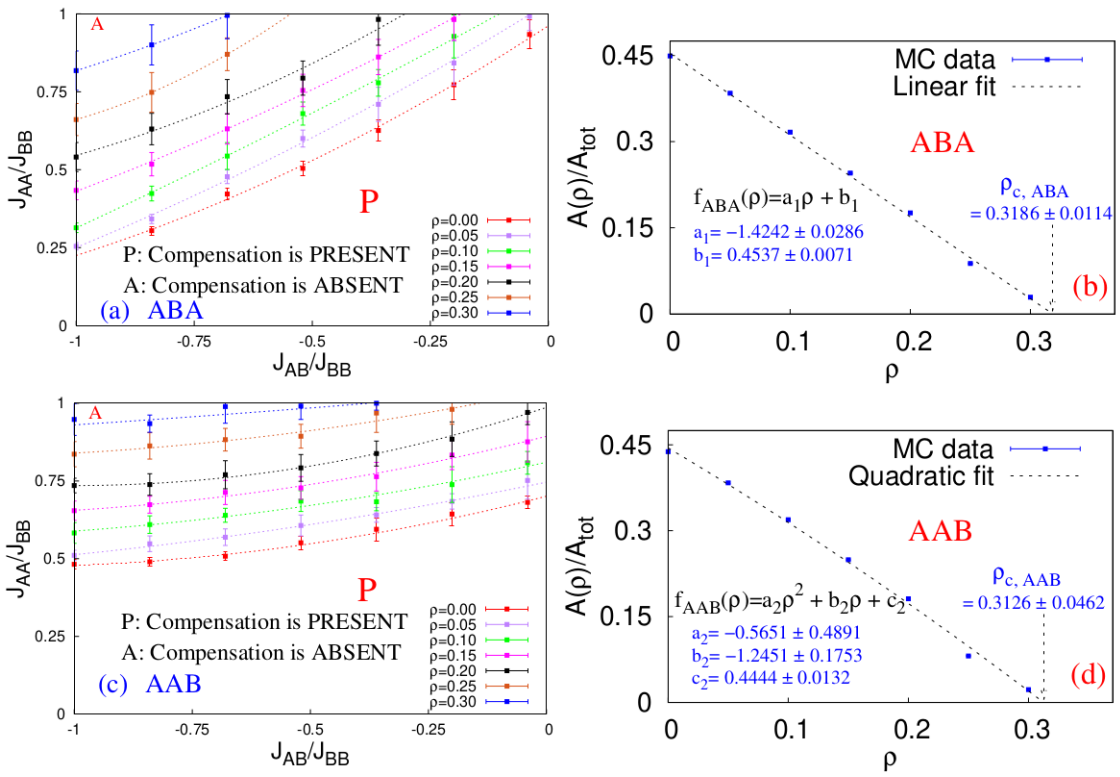

Figure 10: Phase diagrams in the $(J_{AB}/J_{BB} \times J_{AA}/J_{BB})$ plane for: (a) ABA and (c) AAB configurations with concentration of nonmagnetic atoms acting as a parameter. The fractional area of the non-compensating region, $A(\rho)/A_{tot}$, as a function of concentration of non-magnetic impurities, ρ, for, (b) ABA configuration and (d) AAB configuration.

A scaling relation between the magnitude of the phase area without compensation scale with the concentration of the non-magnetic impurities, ρ, is proposed as:

$$\ln \left| \frac{A(\rho)}{\tilde{A}} \right| = a e^{b\rho} \tag{13}$$

type	a	b	$\ln \tilde{A}$	n_{dof}	$\frac{\chi^2}{n_{dof}}$
ABA	-0.1639 ± 0.0294	9.5092 ± 0.5583	-0.6829 ± 0.0574	4	0.0020
AAB	-0.1125 ± 0.0218	10.9771 ± 0.6172	-0.7587 ± 0.0530	4	0.0025

Table 2: Table of scaling parameters of Equation [13] for ABA and AAB trilayer configurations.

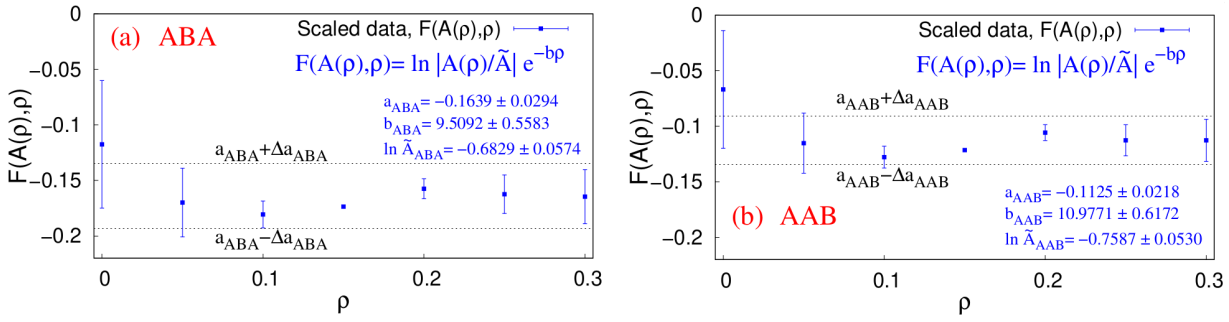

Figure 11: Verification of scaling behaviour of: (A) ABA-type and (B) AAB-type site-diluted square trilayered Ising superlattices.

6 Results, in brief, of nonequilibrium studies

6.1 Effect of a Uniform Random External Magnetic Field with Spatiotemporal Variation on Compensation in Ising Spin-1/2 Trilayered Square Ferrimagnets

The article [28] investigates how disorder affects in trilayered ferrimagnets affects the magnetic and thermodynamic behavior of of ABA- and AAB- type of trilayered stackings of Figure [1], through a uniform random external magnetic field with spatiotemporal variations. The simulations were performed using Monte Carlo simulations, based on the Metropolis algorithm [24], to study the magnetic and thermodynamic responses. The spin configurations were updated based on the Hamiltonians:

$$\begin{aligned} H_{ABA} = & - J_{AA}[\sum_{<t,t'>} S_t^z S_{t'}^z + \sum_{<b,b'>} S_b^z S_{b'}^z] - J_{BB} \sum_{<m,m'>} S_m^z S_{m'}^z \\ & - J_{AB}[\sum_{<t,m>} S_t^z S_m^z + \sum_{<m,b>} S_m^z S_b^z] - \sum_i h_i(t) S_i^z \end{aligned} \tag{14}$$

$$\begin{aligned} H_{AAB} = & - J_{AA}[\sum_{<t,t'>} S_t^z S_{t'}^z + \sum_{<m,m'>} S_m^z S_{m'}^z] - J_{BB} \sum_{<b,b'>} S_b^z S_{b'}^z \\ & - J_{AA} \sum_{<t,m>} S_t^z S_m^z - J_{AB} \sum_{<m,b>} S_m^z S_b^z - \sum_i h_i(t) S_i^z \end{aligned} \tag{15}$$

where $h_i(t)$ is the local, uniform random external magnetic field (at any site, i, at time instant, t) with zero mean and varying standard deviation, σ, is drawn from the following probability distribution:

$$P_{uniform}(h_i(t)) = \begin{cases} \frac{1}{\sqrt{12}\sigma} & |h_i(t)| \leq \sqrt{3}\sigma \\ 0 & |h_i(t)| > \sqrt{3}\sigma \end{cases} \tag{16}$$

The simulations were conducted on a $3 \times 100 \times 100$ lattice with periodic boundary conditions in-plane and open boundary conditions along the vertical axis. The system is initialized at a high temperature and gradually cooled, ensuring steady-state conditions before measurements. Each temperature step consists of 10^5 Monte Carlo sweeps (MCS). For the first cumulative 5×10^4 MCS, the system is allowed to equilibrate in the field-free environment first and then the system attains steady state in the presence of the external field. The exposure time interval is, $\delta = 5 \times 10^4$ MCS.

6.1.1 Results and Discussion

6.1.1.1 Shift in Compensation and Critical Temperatures

As standard deviation, σ, of the external field increases, both compensation and critical temperatures decrease, with the compensation temperature being more sensitive. This shift alters ferrimagnetic behaviors and, in some cases, leads to the disappearance of compensation beyond a threshold value of σ (Figure [12]). The fluctuations of the order parameter (ΔO) and cooperative energy per site (ΔE) demonstrate distinct behaviors in response to increasing σ. The compensation temperature is associated with a smeared peak in the fluctuations, which flattens as σ increases. This further confirms the role of the external field in reducing magnetic order at low temperatures. Lattice morphology analysis at low temperatures shows significant reduction of magnetic order in the A-layers as σ increases (Figure [13] and Figure [14]). In cases where compensation disappears, A layers exhibit nearly random configurations, preventing effective compensation of the system by the B layer's magnetization.

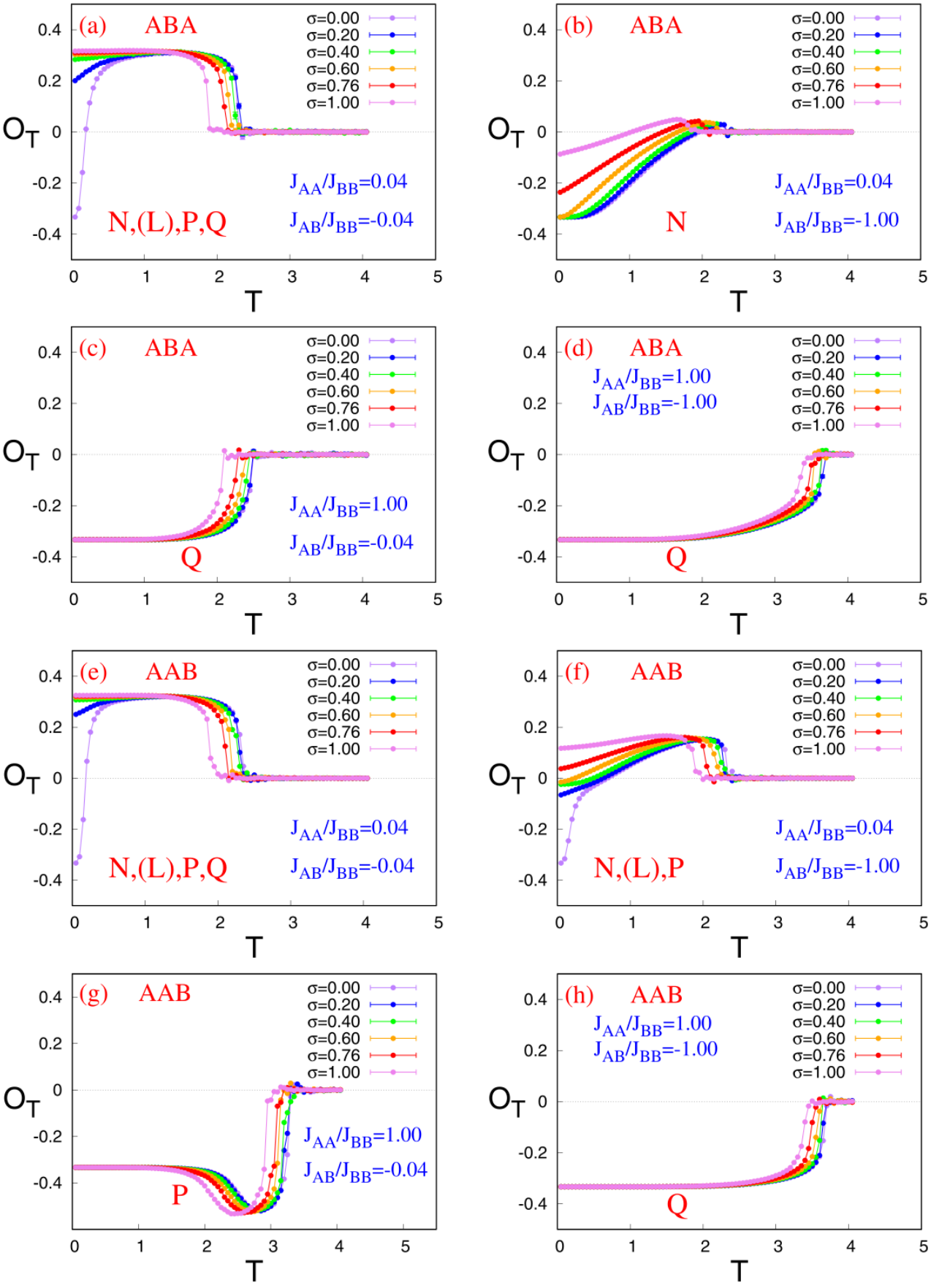

Figure 12: Magnetic response of the trilayered system for a few selected cases with [(a)-(d)] for ABA and [(e)-(h)] for AAB. The shift of both the compensation (where it is present) and critical temperatures toward the low-temperature ends and shift of the magnetic behaviors among N, L, P, and Q, etc., type of ferrimagnetism, with increase in standard deviation of the uniform random external magnetic field, are clearly visible in all these plots. In (a) and (e) we witness the field-driven vanishing of compensation from $\sigma = 0.20$ and upwards.

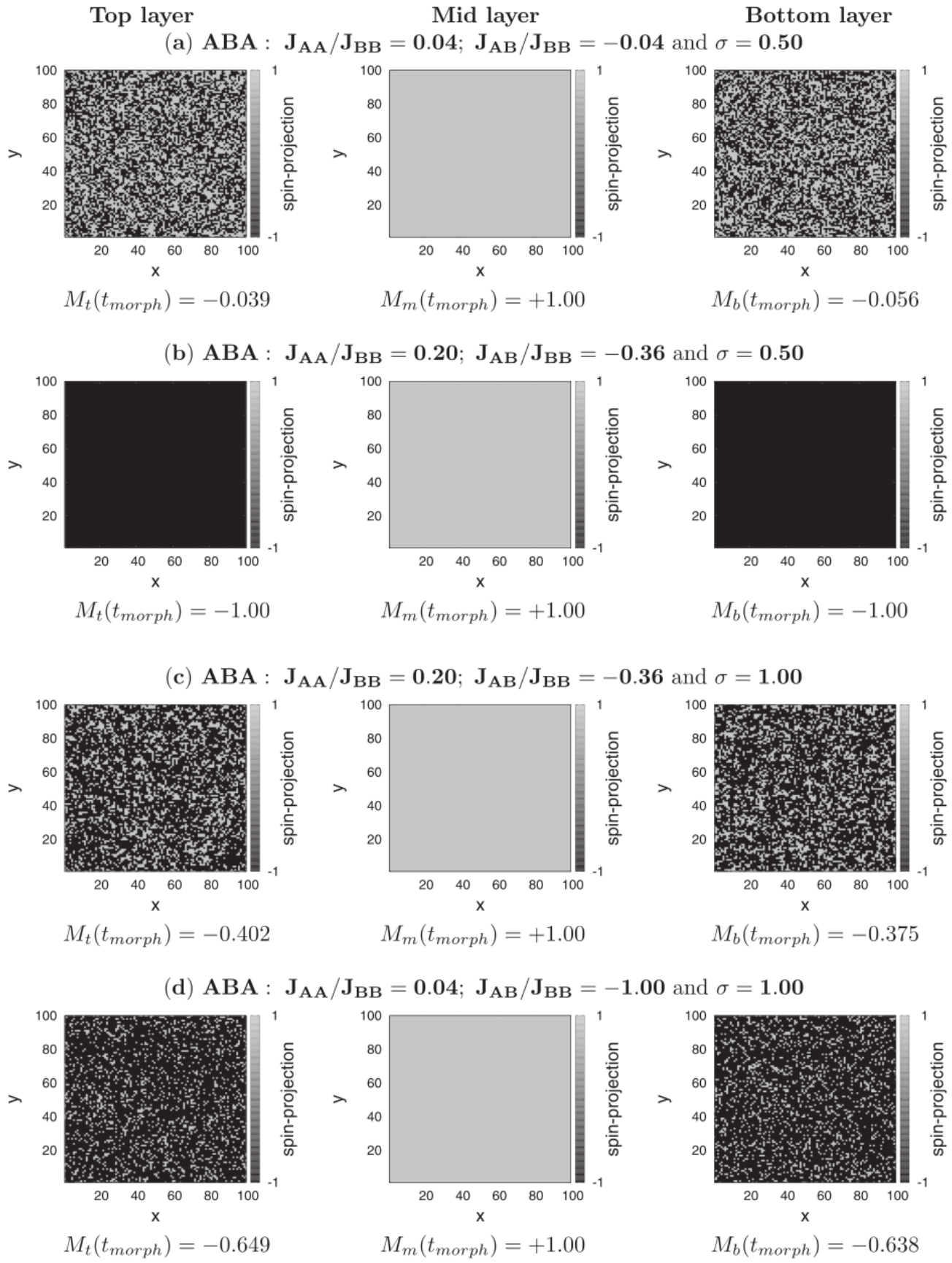
Top layer
Mid layer
Bottom layer
(a) ABA : $J_{AA}/J_{BB} = 0.04$; $J_{AB}/J_{BB} = -0.04$ and $\sigma = 0.50$
$M_t(t_{morph}) = -0.039$
$M_m(t_{morph}) = +1.00$
$M_b(t_{morph}) = -0.056$
(b) ABA : $J_{AA}/J_{BB} = 0.20$; $J_{AB}/J_{BB} = -0.36$ and $\sigma = 0.50$
$M_t(t_{morph}) = -1.00$
$M_m(t_{morph}) = +1.00$
$M_b(t_{morph}) = -1.00$
(c) ABA : $J_{AA}/J_{BB} = 0.20$; $J_{AB}/J_{BB} = -0.36$ and $\sigma = 1.00$
$M_t(t_{morph}) = -0.402$
$M_m(t_{morph}) = +1.00$
$M_b(t_{morph}) = -0.375$
(d) ABA : $J_{AA}/J_{BB} = 0.04$; $J_{AB}/J_{BB} = -1.00$ and $\sigma = 1.00$
$M_t(t_{morph}) = -0.649$
$M_m(t_{morph}) = +1.00$
$M_b(t_{morph}) = -0.638$
x
y
spin-projection

Figure 13: For the ABA configuration: Lattice morphologies of the top layer (left); middle layer (middle), and the bottom layer (right) at $t = t_{morph} = 10^5$ MCS for a few selected coupling strengths and external field. The destruction of compensation in the cases (a) and (c) is due to the significant reduction of magnetic ordering in the top and bottom layers, i.e., surface layers.

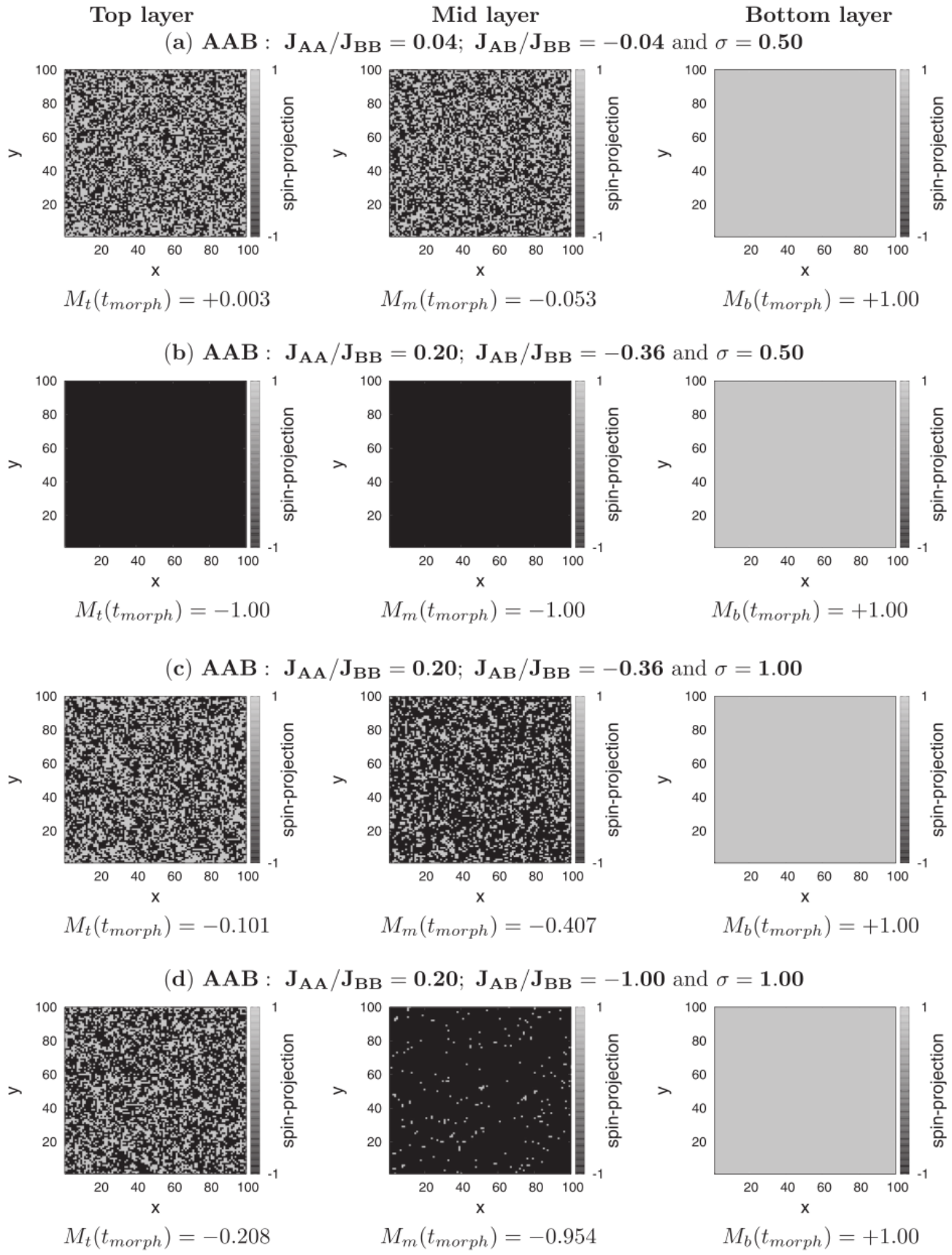
Top layer
Mid layer
Bottom layer
(a) AAB : $J_{AA}/J_{BB} = 0.04$; $J_{AB}/J_{BB} = -0.04$ and $\sigma = 0.50$
$M_t(t_{morph}) = +0.003$
$M_m(t_{morph}) = -0.053$
$M_b(t_{morph}) = +1.00$
(b) AAB : $J_{AA}/J_{BB} = 0.20$; $J_{AB}/J_{BB} = -0.36$ and $\sigma = 0.50$
$M_t(t_{morph}) = -1.00$
$M_m(t_{morph}) = -1.00$
$M_b(t_{morph}) = +1.00$
(c) AAB : $J_{AA}/J_{BB} = 0.20$; $J_{AB}/J_{BB} = -0.36$ and $\sigma = 1.00$
$M_t(t_{morph}) = -0.101$
$M_m(t_{morph}) = -0.407$
$M_b(t_{morph}) = +1.00$
(d) AAB : $J_{AA}/J_{BB} = 0.20$; $J_{AB}/J_{BB} = -1.00$ and $\sigma = 1.00$
$M_t(t_{morph}) = -0.208$
$M_m(t_{morph}) = -0.954$
$M_b(t_{morph}) = +1.00$
x
y
spin-projection

Figure 14: For the AAB configuration: Lattice morphologies of the top layer (left), middle layer (middle), and bottom layer (right) at $t = t_{morph} = 10^5$ MCS for a few selected coupling strengths and external field. The destruction of compensation in the cases (a) and (c) is due to the significant reduction of magnetic ordering in the top and bottom layers, i.e., surface layers.

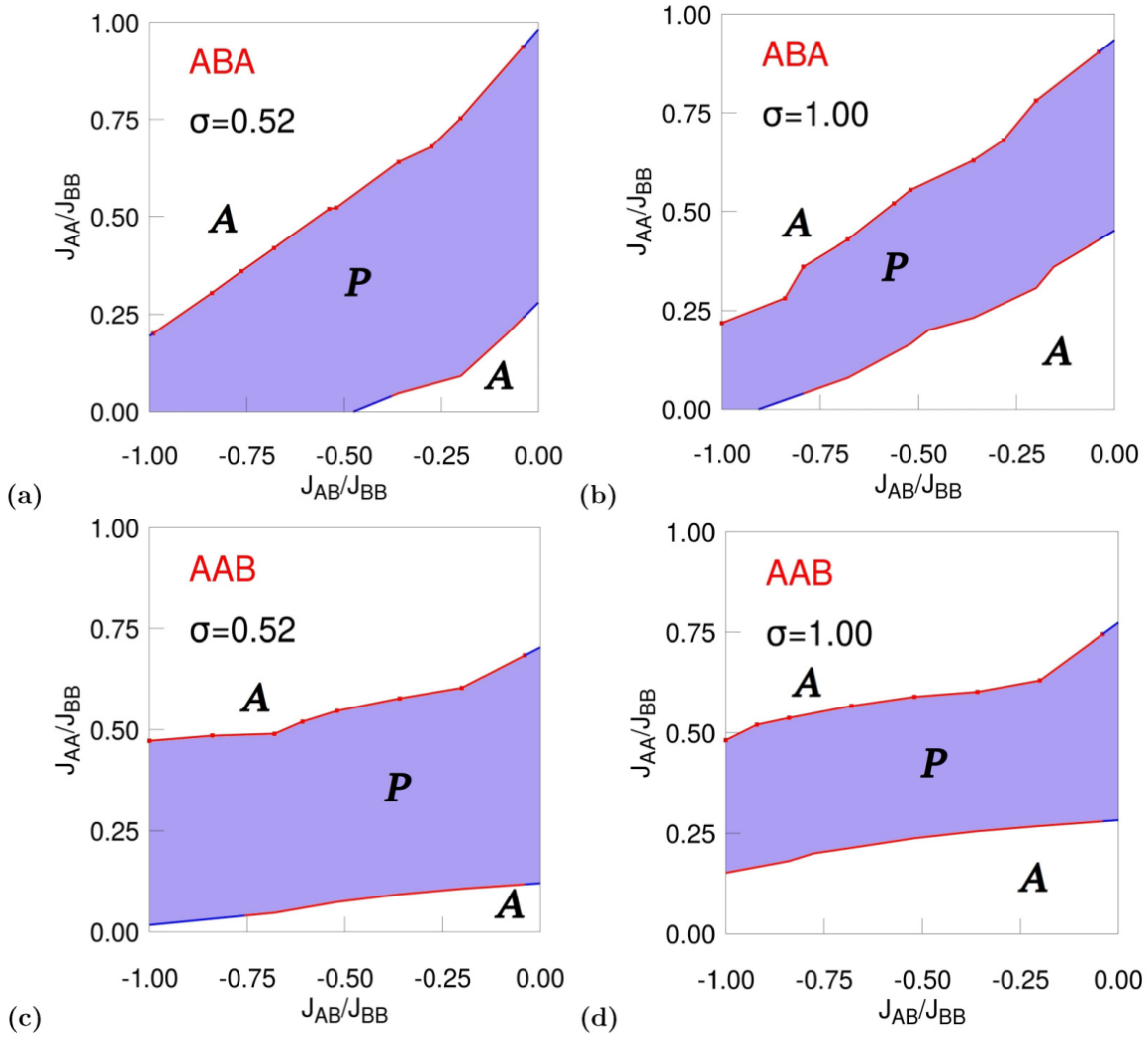

Figure 15: Phase diagram for the ABA trilayered ferrimagnetic system when (a) $\sigma = 0.52$, (b) $\sigma = 1.00$, and AAB trilayered ferrimagnetic system when (c) $\sigma = 0.52$ and (d) $\sigma = 1.00$, in presence of the uniform random external magnetic field. A: Compensation is absent; P: compensation is present.

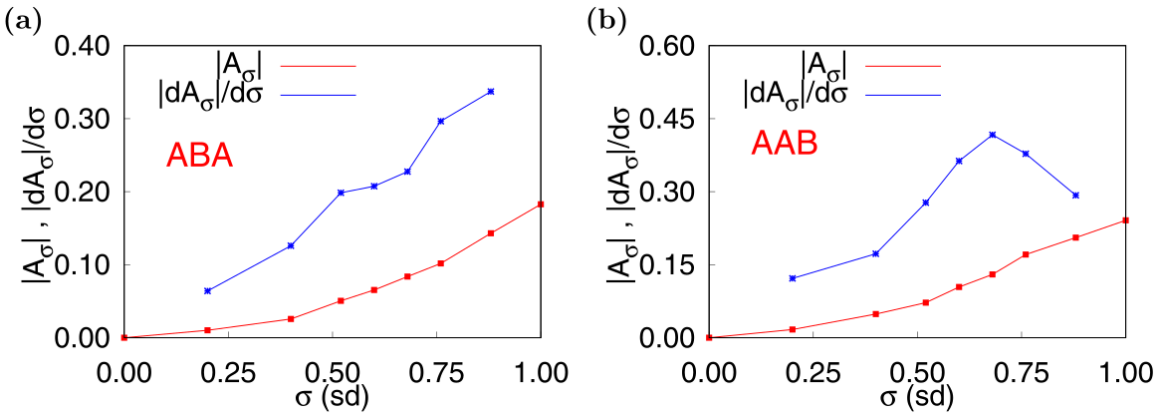

Figure 16: Plots of magnitude of the area of the no-compensation islands versus standard deviation of the field (red) and the rate of increase in the magnitude of the area of the no-compensation islands versus standard deviation of the external uniform magnetic field (blue) for the (a) ABA and (b) AAB configurations.

6.1.1.2 Field-Driven Absence of Compensation

For certain combinations of coupling strengths and field strengths, the compensation phenomenon vanishes. The mechanism behind this phenomenon is attributed to the randomization of A-layers'

magnetic ordering due to strong spin-field interaction energies. When the spin-field energies exceed the cooperative energies, sublattice magnetizations of A layers become insufficient to cancel the magnetization of the B layer, leading to the absence of compensation. Phase diagrams reveal the formation of islands where compensation is absent within regions where compensation exists in the field-free case (Figure 15). The size of these islands increases with σ (Figure 16). A scaling relation is proposed:

$$f(A(\sigma), \sigma) = \sigma^{-b} A(\sigma) \tag{17}$$

where the exponents are found to be $b_{ABA} = 1.958 \pm 0.122$ and $b_{AAB} = 1.783 \pm 0.118$.

6.2 Effect of a Gaussian Random External Magnetic Field with Spatiotemporal Variation on Compensation in Ising Spin-1/2 Trilayered Square Ferrimagnets

The *Monte Carlo simulations*, in this study [29], is performed on the pristine ABA and AAB trilayered configurations (Figure 1). The disorder, introduced by the external Gaussian field, affects the compensation and critical temperatures, and in some cases, completely eliminate the compensation effect. Each site of a trilayered Ising ferrimagnet possesses an intrinsic spin value $\pm 1/2$. The simulations were performed using Monte Carlo simulations, based on the Metropolis algorithm [24], to study the magnetic and thermodynamic responses of a system size of $(3 \times 100 \times 100)$. The spin configurations were updated based on the Hamiltonians:

$$\begin{aligned} H_{ABA} = & - J_{AA}[\sum_{<t,t'>} S_t^z S_{t'}^z + \sum_{<b,b'>} S_b^z S_{b'}^z] - J_{BB} \sum_{<m,m'>} S_m^z S_{m'}^z \\ & - J_{AB}[\sum_{<t,m>} S_t^z S_m^z + \sum_{<m,b>} S_m^z S_b^z] - \sum_i h_i(t) S_i^z \end{aligned} \tag{18}$$

$$\begin{aligned} H_{AAB} = & - J_{AA}[\sum_{<t,t'>} S_t^z S_{t'}^z + \sum_{<m,m'>} S_m^z S_{m'}^z] - J_{BB} \sum_{<b,b'>} S_b^z S_{b'}^z \\ & - J_{AA} \sum_{<t,m>} S_t^z S_m^z - J_{AB} \sum_{<m,b>} S_m^z S_b^z - \sum_i h_i(t) S_i^z \end{aligned} \tag{19}$$

where $h_i(t)$ is the local, Gaussian random external magnetic field (at any site, i, at time instant, t) with zero mean and varying standard deviation, σ, is drawn from the following probability distribution:

$$P(h_i) = \frac{1}{\sqrt{2\pi\sigma^2}} \exp\left(\frac{-h_i^2}{2\sigma^2}\right) \tag{20}$$

where σ is the standard deviation of the field. Box-Muller algorithm [36] is used to get a Gaussian distribution. One such distribution G_0 of standard deviation, σ and zero mean can be obtained from two uniform random distributions U_1 and U_2, between $[0, 1]$ from the following equation:

$$G_0 = \sigma\sqrt{-2\ln U_1} cos(2\pi U_2) \tag{21}$$

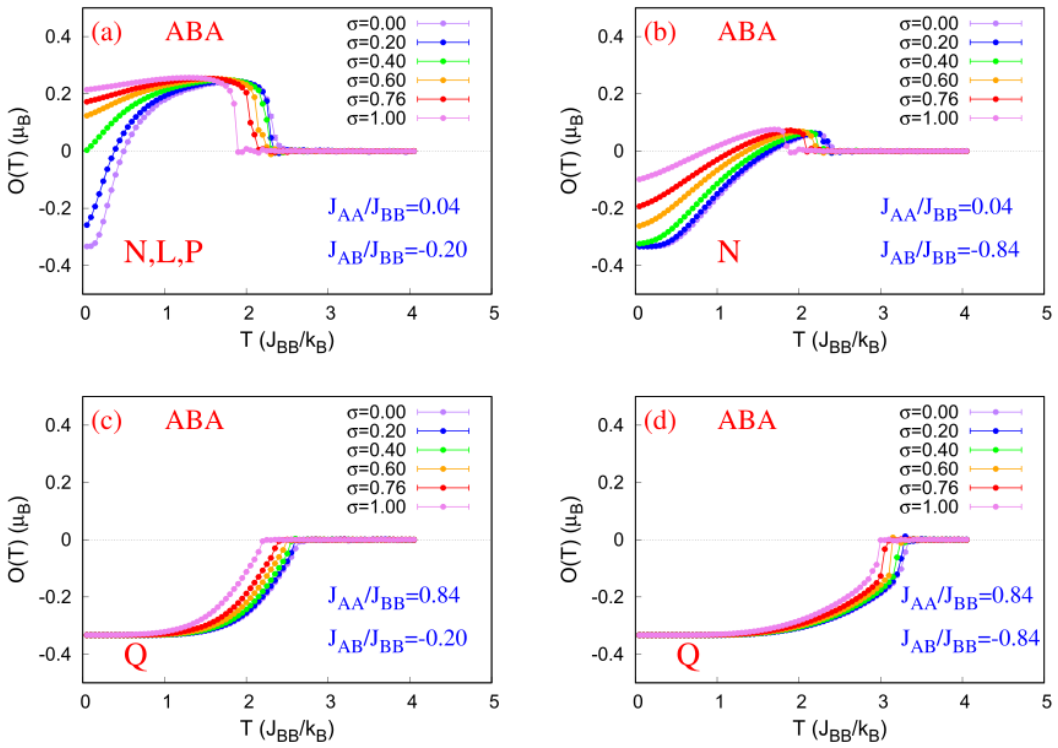

Figure 17: Magnetic response of the trilayered system for a few selected cases with [(a)-(d)] ABA. The shift of both the compensation (where it is present) and critical temperatures toward the low-temperature ends and shift of the magnetic behaviors among N, L, P, and Q, etc., type of ferrimagnetism, with increase in standard deviation of the Gaussian random external magnetic field, are clearly visible in all these plots. We witness the field-driven vanishing of compensation from $\sigma = 0.20$ and upwards.

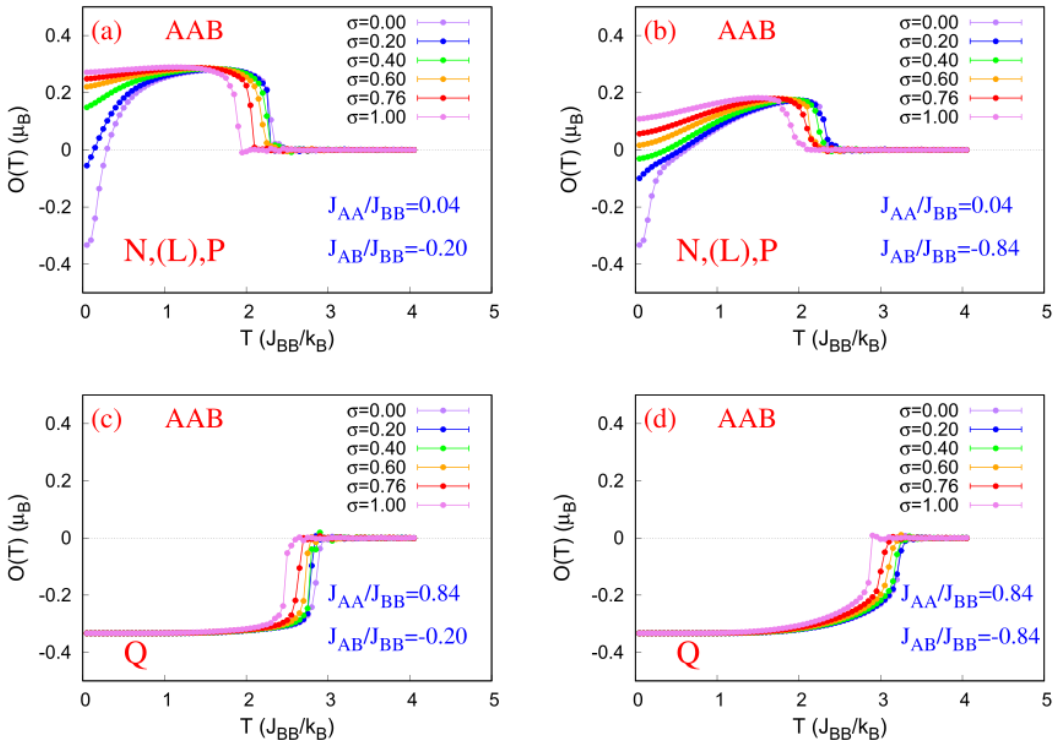

Figure 18: Magnetic response of the trilayered system for a few selected cases with [(a)-(d)] AAB. The shift of both the compensation (where it is present) and critical temperatures toward the low-temperature ends and shift of the magnetic behaviors among N, L, P, and Q, etc., type of ferrimagnetism, with increase in standard deviation of the Gaussian random external magnetic field, are clearly visible in all these plots. We witness the field-driven vanishing of compensation from $\sigma = 0.20$ and upwards.

Periodic boundary conditions in-plane, and open boundary conditions along the vertical are used. The system is initialized at high temperature and gradually cooled, ensuring steady-state conditions before measurements. Each temperature step consists of 10^5 Monte Carlo sweeps (MCS). For the first cumulative 5×10^4 MCS, the system is allowed to equilibrate in the field-free environment first and then the system attains steady state in the presence of the external field. The exposure time interval is, $\delta = 5 \times 10^4$ MCS. For each parameter set of ferromagnetic interaction strength: J_{AA}/J_{BB}, antiferromagnetic interaction strength: J_{AB}/J_{BB} and Standard deviation of the external field: σ; the sublattice magnetizations, total magnetization, order parameters, and fluctuations are computed.

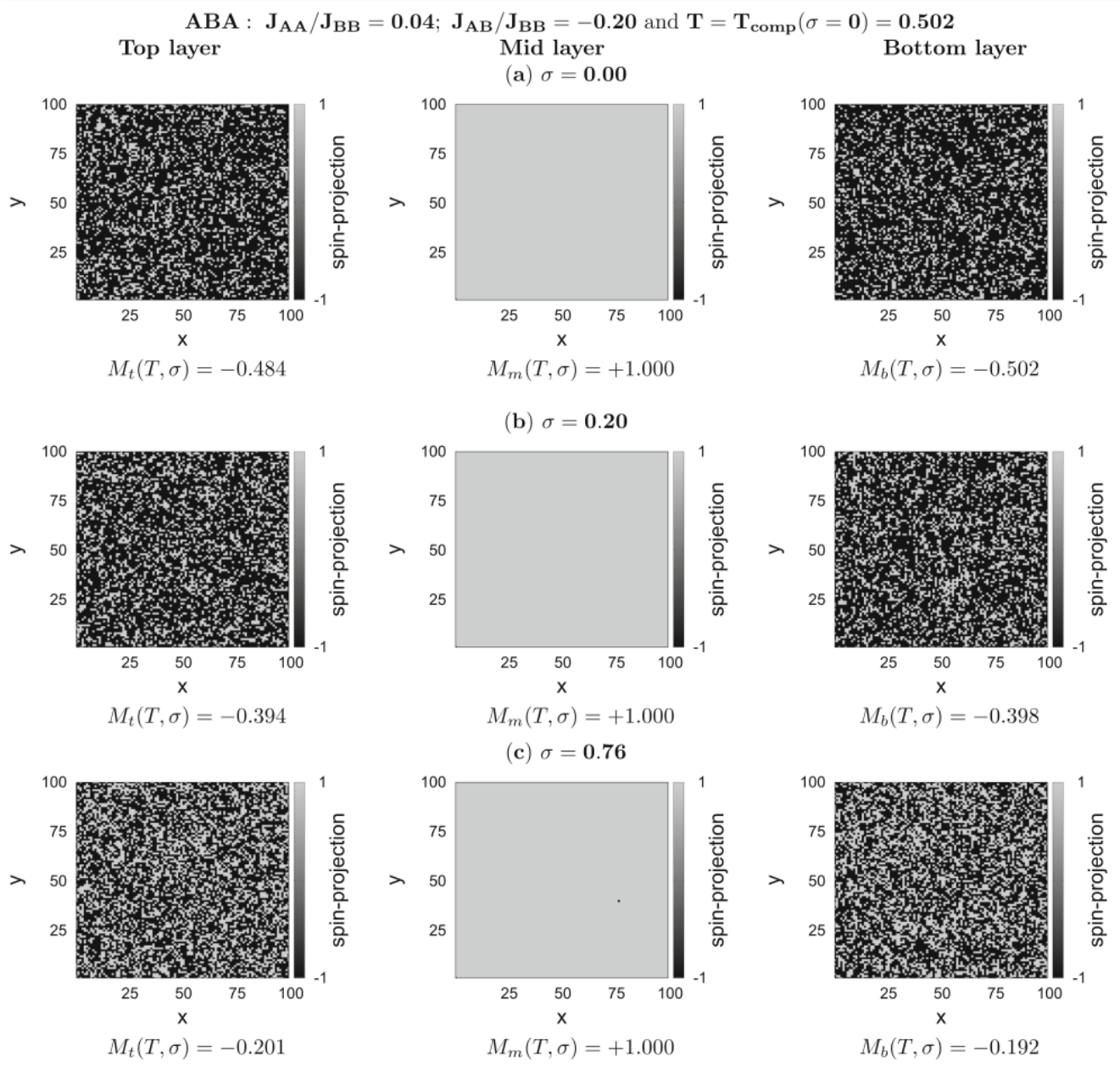

Figure 19: For the ABA configuration: Lattice morphologies of the top layer (left); middle layer (middle), and the bottom layer (right) at $t = t_{morph} = 10^5$ MCS for a few selected coupling strengths and external field. The destruction of compensation in the cases (a) and (c) is due to the significant reduction of magnetic ordering in the top and bottom layers, i.e., surface layers.

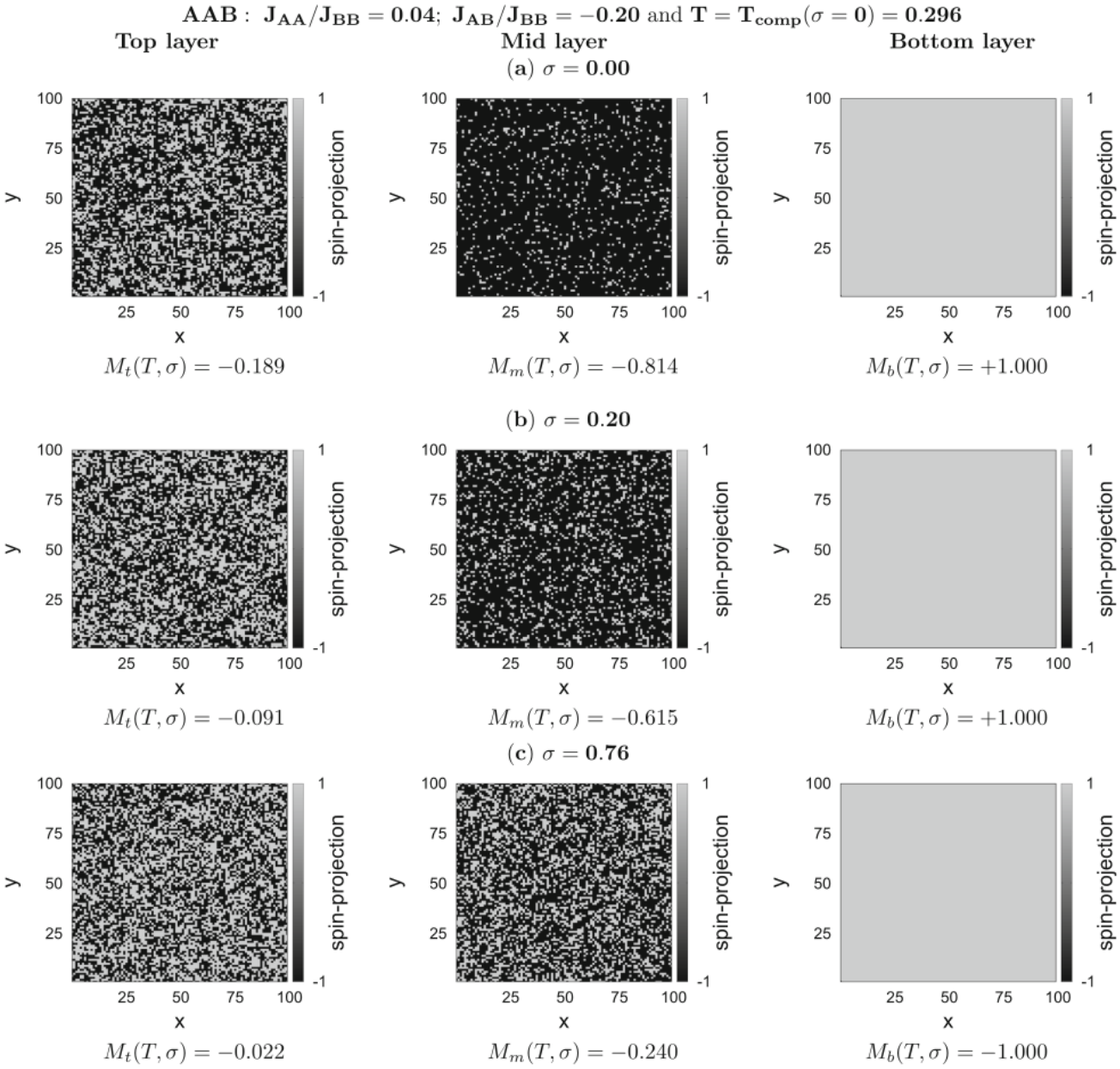

Figure 20: For the ABA configuration: Lattice morphologies of the top layer (left); middle layer (middle), and the bottom layer (right) at $t = t_{morph} = 10^5$ MCS for a few selected coupling strengths and external field. The destruction of compensation in the cases (a) and (c) is due to the significant reduction of magnetic ordering in the top and bottom layers, i.e., surface layers.

6.2.1 Results and Discussion

6.2.1.1 Magnetization vs. Temperature

Increasing field randomness lowers the compensation and critical temperatures, and the temperature dependence of magnetization reveals different ferrimagnetic behaviors categorized as P-type, N-type, L-type, and Q-type etc. For weak coupling strengths, compensation disappears at a critical σ, as the magnetic ordering in A-layers weakens, preventing them from canceling the magnetization of the B-layer. Peaks in fluctuations in the order parameter and cooperative energy provide insights into compensation loss. As randomness increases, peaks broaden and decrease in magnitude, signifying a suppression of compensation behavior.

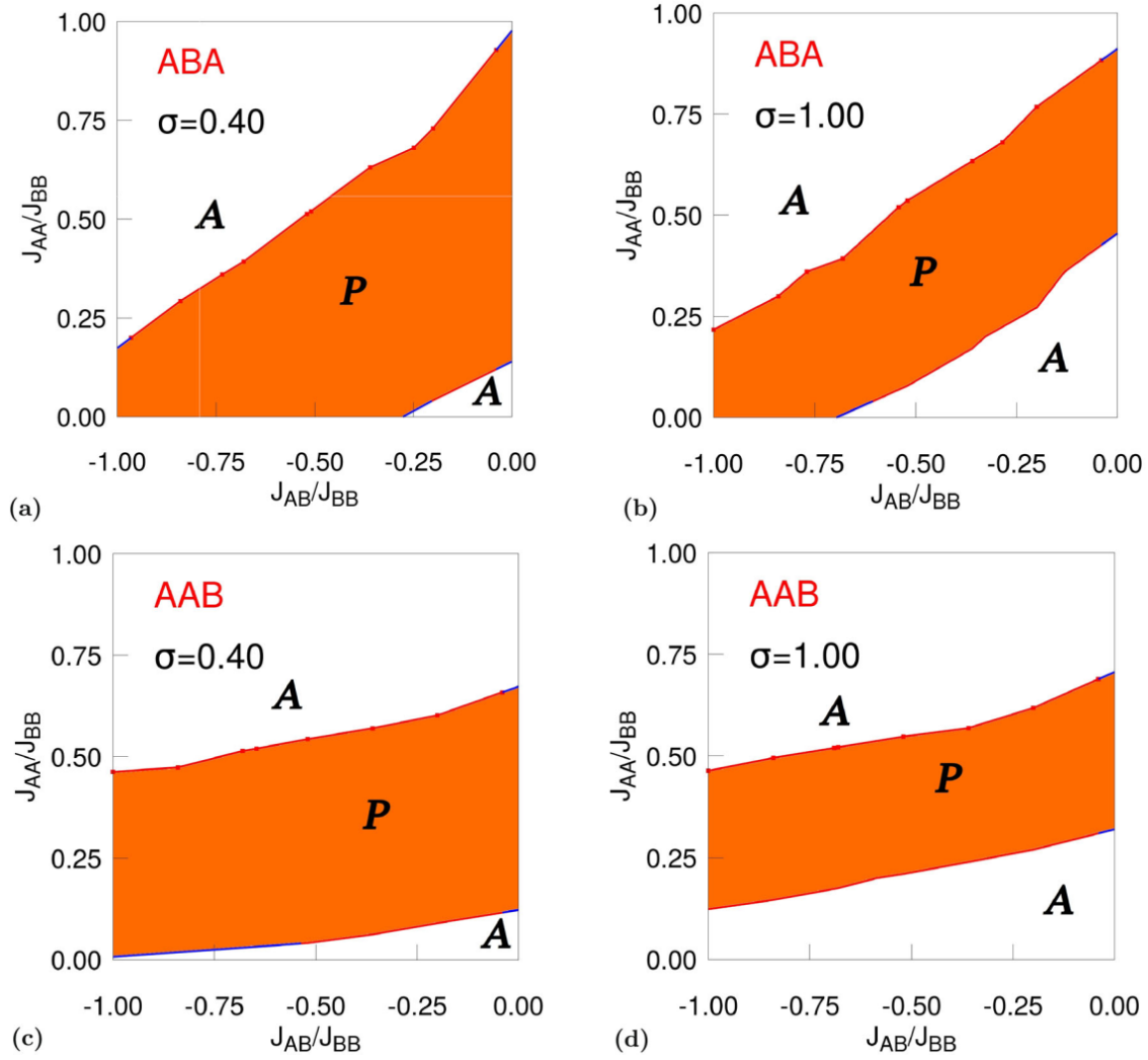

Figure 21: Phase diagram for the ABA trilayered ferrimagnetic system when (a) $\sigma = 0.52$, (b) $\sigma = 1.00$, and AAB trilayered ferrimagnetic system when (c) $\sigma = 0.52$ and (d) $\sigma = 1.00$, in presence of the Gaussian random external magnetic field. A: Compensation is absent; P: compensation is present.

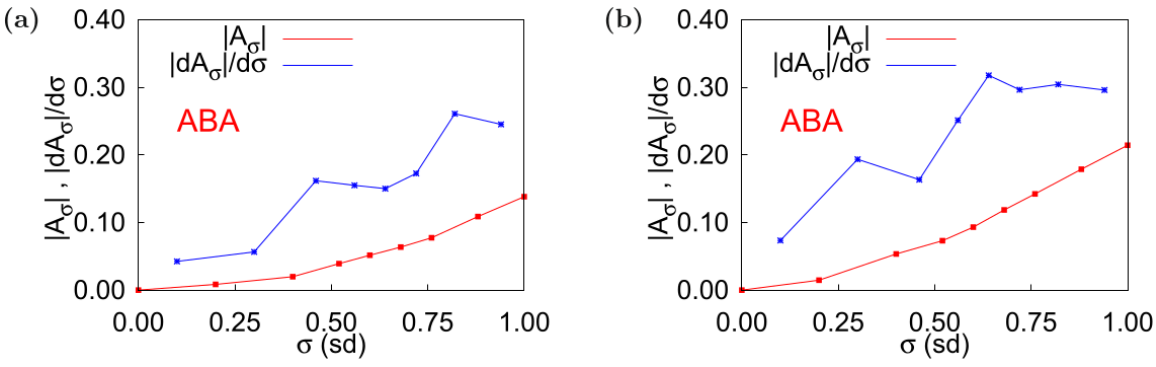

Figure 22: Plots of magnitude of the area of the no-compensation islands versus standard deviation of the Gaussian random field (red) and the rate of increase in the magnitude of the area of the no-compensation islands versus standard deviation of the Gaussian random field (blue) for the (a) ABA and (b) AAB configurations.

6.2.1.2 Phase Diagram and Scaling

The phase diagrams constructed reveal the emergence of "no-compensation" islands (NCIs), where compensation vanishes within an otherwise magnetically compensated region. No-compensation islands

(NCIs) emerge and grow with increasing σ, following the scaling relation:

$$f(A(\sigma), \sigma) = \sigma^{-b} A(\sigma) \tag{22}$$

where the exponents are found to be $b_{ABA} = 1.913 \pm 0.137$ and $b_{AAB} = 1.625 \pm 0.066$.

7 Conclusion and future directions

The equilibrium studies [25,26] provide us with analytical and empirical relations for IARRM and ΔT, which enable us in predicting compensation in ferrimagnetic trilayered, ABA and AAB configurations, *without exhaustive simulations*. The fitted phase diagrams, are quantitatively similar to the ones obtained by MC simulation. The work, in [27], establishes that site dilution in trilayered square ferrimagnets, of type ABA and AAB, significantly affects compensation phenomena. Monte Carlo simulations reveal impurity-driven creation of compensation points, can be engineered by appropriately tuning coupling ratios and impurity levels, making these materials highly adaptable for technological applications.

The non-equilibrium studies [28,29] demonstrate that external random fields significantly modify the compensation behavior of trilayered Ising ferrimagnets. Key findings include:
(a) Compensation and critical temperatures shift towards lower temperature values with increasing randomness.
(b) Compensation disappears beyond a critical standard deviation (σ) of the external magnetic field, due to reduced magnetic ordering. Dynamic vanishing of compensation results from the competition between cooperative and spin-field energies.
(c) For both the uniform and Gaussian random fields, values of scaling exponent overlap, within statistical interval, indicating that compensation loss is primarily driven by randomness rather than the type of field distribution.

Future studies could investigate the effects of randomness in layer compositions, the impact of external magnetic fields, and the integration of layered structures into device applications.

References

[1] Geim A. K., & Novoselov K. S., *Nat. Mater.* **6**, 183 (2007).

[2] Gong C., Li L., Li Z., Ji H., Stern A., et al., *Nature* **546 (7657)**, 265 (2017).

[3] Huang B., Clark G., Navarro-Moratalla E., Klein D. R., Cheng R., et al., *Nature* **546 (7657)**, 270 (2017).

[4] Song T., Fei Z., Yankowitz M., Lin Z., Jiang Q., et al., *Nat. Mater.* **18**, 1298 (2019).

[5] Geim A. K., & Grigorieva I. V., *Nature* **499**, 419 (2013).

[6] McGuire M. A., *Crystals* **7 (5)**, 121 (2017).

[7] Ouvrard G., Brec R., & Rouxel J., *Mater. Res. Bull.* **20(10)**, 1181 (1985).

[8] Kim K., Park K., Son S., Park C. -H., Lim S. Y., et al., *2D Mater.* **6 (4)**, 041001 (2019).

[9] Lee J. U., Lee S., Ryoo J. H., Kang S., Kim T. Y., et al., *Nano Lett.* **16**, 7433 (2016).

[10] Taylor B., Steger J., Wold A., & Kostiner E., *Inorg. Chem.*, **13**, 2719 (1974).

[11] Wiedenmann A., Rossat-Mignod J., Louisy A., Brec R., & Rouxel J., *Solid State Commun.* **40**, 1067 (1981).

[12] Carteaux V., Moussa F., & Spiesser M., *Europhys. Lett.* **29**, 251 (1995).

[13] Fei Z., Huang B., Malinowski P., Wang W., Song T., et al., *Nat. Mater.* **17**, 778 (2018).

[14] Mak K. F., Shan J., & Ralph D. C., *Nat. Rev. Phys.* **1**, 646 (2019).

[15] Gong S. J., and Gong C., *Nat. Nanotechnol.* (2025). https://doi.org/10.1038/s41565-025-01884-6

[16] Néel M. L., *Ann. de Phys.* **12**, 137 (1948).

[17] Cullity B. D., and Graham C. D., Introduction to Magnetic Materials, 2nd edn. (Wiley, New York, 2008)

[18] Diaz I. J. L., and Branco N. S., *Phys. B* **529**, 73 (2018).

[19] Diaz I. J. L., and Branco N. S., *Phys. A* **540**, 123014 (2019).

[20] Diaz I. J. L., and Branco N. S., *Phys. A* **468**, 158 (2017).

[21] Balcerzak T., and Szałowski K., *Phys. A* **395**, 183 (2014).

[22] Szałowski K., and Balcerzak T., *J. Phys.: Condens. Matter* **26**, 386003 (2014).

[23] Diaz I. J. L., and Branco N. S., *Phys. A* **490**, 904 (2018).

[24] Metropolis N., Rosenbluth A. W., Rosenbluth M. N., Teller A. H., and Teller E., *J. Chem. Phys.* **21**, 1087 (1953).

[25] Chandra S., and Acharyya M., *AIP Conf. Proc.* **2220**, 130037 (2020).

[26] Chandra S., *Eur. Phys. J. B* **94(1)**, 13 (2021).

[27] Chandra S., unpublished manuscript, *(In Communication)*.

[28] Chandra S., *Phys. Rev. E* **104**, 064126 (2021).

[29] Chandra S., *Eur. Phys. J. Plus* **138**, 573 (2023)

[30] Anagnostopoulos K. N., *Computational Physics* (National Technical University of Athens, 2014).

[31] Yeomans J. M., *Statistical Mechanics of Phase Transitions* (Oxford University Press, New York, 1992).

[32] Ising E., *Z. Phys.* **31(1)**, 253 (1925).

[33] Grünberg P. et al., *Phys. Rev. Lett.* **57**, 2442 (1986).

[34] Phan M. -H., and Yu S. -C., *J. Magn. Magn. Mater.* **308**, 325 (2007).

[35] Binder K., *Phys. Rev. Lett.* **47**, 693 (1981).

[36] Box G. E. P., and Muller M. E., *Ann. Math. Statist.* **29(2)**, 610 (1958).

List of Publications

Publications included in this thesis

1. Chandra S., and Acharyya M., A Monte Carlo study on the variation of residual magnetisation with the ratio of coupling strengths and non-magnetic impurities in an Ising trilayer, *AIP Conference Proceedings* **2220**, 130037 (2020)

2. Chandra S., Thermodynamic behaviour of magnetocaloric quantities in spin-1/2 Ising square trilayer, *The European Physical Journal B* **94(1)**, 13 (2021)

3.Chandra S., Optimizing Compensation in Ising Spin-1/2 site-diluted Trilayered Square Ferrimagnets: Insights from Monte Carlo Simulations, *(In Communication)*

4. Chandra S., Effect of a uniform random external magnetic field with spatiotemporal variation on compensation in Ising spin-1/2 trilayered square ferrimagnets, *Physical Review E* **104**, 064126 (2021)

5. Chandra S., Effect of a Gaussian random external magnetic field with spatio temporal variation on compensation in Ising spin-1/2 trilayered square ferrimagnets, *The European Physical Journal Plus* **138**, 573 (2023)

Publications not included in this thesis

6. Chandra S., Compensation and its systematics in spin-1/2 Ising trilayered triangular ferrimagnet, *Journal of Physics and Chemistry of Solids* **156**, 110165 (2021)

7. Banerjee P. and Chandra S., A Metropolis study of the isothermal magnetic entropy change in spin-1/2 Ising model, *Materials Today: Proceedings* **55(P1)**, 7 (2022)

8. Chandra S., A Monte Carlo study on the temperature dependence of hysteresis loops in Ising Spin-1 Square Bilayers, *Materials Today: Proceedings* **66(P7)**, 3238 (2022)

9. Chandra S., Effects of site dilution on Compensation in Ising Spin-1/2 trilayered triangular Ferrimagnets with non-equivalent planes, *Physica A* **619**, 128737 (2023)